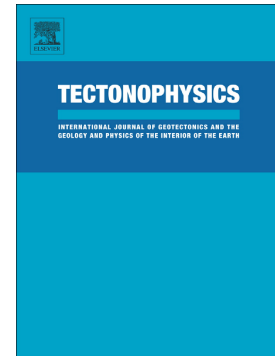


## Accepted Manuscript

Active faulting in the central Betic Cordillera (Spain):  
Palaeoseismological constraint of the surface-rupturing history of  
the Baza Fault (Central Betic Cordillera, Iberian Peninsula)

J. Castro, I. Martin-Rojas, I. Medina-Cascales, F.J. García-  
Tortosa, P. Alfaro, J.M. Insua-Arévalo



PII: S0040-1951(18)30145-8  
DOI: doi:[10.1016/j.tecto.2018.04.010](https://doi.org/10.1016/j.tecto.2018.04.010)  
Reference: TECTO 127822  
To appear in: *Tectonophysics*  
Received date: 21 September 2017  
Revised date: 30 March 2018  
Accepted date: 6 April 2018

Please cite this article as: J. Castro, I. Martin-Rojas, I. Medina-Cascales, F.J. García-Tortosa, P. Alfaro, J.M. Insua-Arévalo , Active faulting in the central Betic Cordillera (Spain): Palaeoseismological constraint of the surface-rupturing history of the Baza Fault (Central Betic Cordillera, Iberian Peninsula). The address for the corresponding author was captured as affiliation for all authors. Please check if appropriate. Tecto(2017), doi:[10.1016/j.tecto.2018.04.010](https://doi.org/10.1016/j.tecto.2018.04.010)

This is a PDF file of an unedited manuscript that has been accepted for publication. As a service to our customers we are providing this early version of the manuscript. The manuscript will undergo copyediting, typesetting, and review of the resulting proof before it is published in its final form. Please note that during the production process errors may be discovered which could affect the content, and all legal disclaimers that apply to the journal pertain.

**Active faulting in the central Betic Cordillera (Spain): Palaeoseismological  
constraint of the surface-rupturing history of the Baza Fault (Central  
Betic Cordillera, Iberian Peninsula)**

**Castro, J. <sup>1</sup>; Martin-Rojas, I. <sup>1</sup>; Medina-Cascales, I. <sup>1</sup>; García-Tortosa, F.J. <sup>2</sup>; Alfaro, P. <sup>1</sup>  
and Insua-Arévalo, J.M. <sup>3</sup>**

1 Dpto. Ciencias de la Tierra y del Medio Ambiente, Universidad de Alicante. Ctra de  
San Vicente del Raspeig, s/n, 03690- Alicante. julia.castro@ua.es

2 Dpto. Geología, Universidad de Jaén. Campus Las Lagunillas, s/n, 23071 Jaén.  
gtortosa@ujen.es

3 Dpto de Geodinámica, Facultad de Geología. Universidad Complutense de Madrid,  
Spain.

**Key words:** Active Tectonics, Palaeoseismicity, Recurrence Interval, Baza Fault

**ABSTRACT**

This paper on the Baza Fault provides the first palaeoseismic data from trenches in the central sector of the Betic Cordillera (S Spain), one of the most tectonically active areas of the Iberian Peninsula.

With the palaeoseismological data we constructed time-stratigraphic OxCal models that yield probability density functions (PDFs) of individual palaeoseismic event timing. We analysed PDF overlap to quantitatively correlate the walls and site events into a single earthquake chronology. We assembled a surface-rupturing history of the Baza Fault for the last ca. 45000 years. We postulated six alternative surface rupturing histories including 8-9 fault-wide earthquakes. We calculated fault-wide earthquake recurrence intervals using Monte Carlo. This analysis yielded a 4750-5150 yr recurrence interval. Finally, compared our results with the results from empirical relationships.

Our results will provide a basis for future analyses of more of other active normal faults in this region. Moreover, our results will be essential for improving earthquake-probability assessments in Spain, where palaeoseismic data are scarce.

## 1. INTRODUCTION

The central Betic Cordillera is the most active tectonic zone of the Iberian Peninsula (Sanz de Galdeano et al., 2012 and references therein), with the highest seismic hazard, according to the Spanish Building Code. Several significant historical earthquakes took place in this central sector of the Cordillera, including the 1884 Andalusian earthquake ( $I_{EMS98}$  IX-X / estimated magnitude  $M_w = 6.5$ ) (Muñoz and Udías, 1991) and the 1531 Baza earthquake ( $I_{MMI}$  VIII-IX; estimated magnitude ca. 6.0) (Martínez-Solares and Mezcua, 2003; Sanz de Galdeano et al., 2012). In addition, this central sector of the Betic Cordillera has the highest instrumental seismicity rate of the Iberian Peninsula (Sanz de Galdeano and Peláez, 2011), especially in the Granada basin.

This seismicity is related to a geodynamic setting characterised by regional NW-SE compression and an approximately orthogonal ENE-WSW tension (Galindo-Zaldívar et al., 1999; Herráiz et al., 2000; Stich et al., 2006; De Vicente et al., 2008; Martín et al., 2015). Regional ENE-WSW extension is accommodated by several NW-SE normal faults, such as the Granada fault system (Gil et al., 2002; Ruiz et al., 2003; Rodríguez-Fernández and Sanz de Galdeano, 2006, among others) or the Baza Fault (Alfaro et al., 2008). Despite good geomorphological expression of these normal faults (Lhénaff, 1965; Estévez and Sanz de Galdeano, 1983; Riley and Moore, 1993; Calvache et al., 1997; García-Tortosa et al., 2008, 2011), palaeoseismological information is scarce. Reicherter (2001) cites the occurrence of at least three earthquakes in the Ventas de Zafarraya fault (seismogenic source of the 1884 Andalusian earthquake) during the last 9000 yr in the westernmost sector of the Granada basin. Alfaro et al. (2001) show evidence of recent



tectonic activity of the Padul fault, describing palaeoliquefaction structures in Upper Pleistocene sediments in the Padul-Nigüelas basin located in the hangingwall of the Padul fault. Although these results are informative, the palaeoseismic record of the active faults of this region is, at present, very poor and is even absent in the Guadix-Baza basin (our study area).

It is well known that the farther the record can be extended back in time, the more realistic the palaeoseismic assessments will be, especially when dealing with slow faults with long recurrence intervals. In these cases, seismic hazard assessments based exclusively on historic and instrumental records present limited reliability, and they must be improved by incorporating palaeoseismological data (Reiter 1990, 1995).

In the case of the Baza Fault, one of the most active faults of the central Betic Cordillera (Sanz de Galdeano et al., 2012), no palaeoseismic data have been reported until now. Only indirect evidence of seismic activity has been reported through palaeoliquefaction features in Pleistocene sediments (Alfaro et al., 1997; 2010).

The goal of this study is to present the first field and palaeoseismological evidence from the Baza Fault that includes geological and geomorphic characterization along the fault trace, together with trench digging and analysis. These data lead us to propose a preliminary surface rupturing history for the last ca. 45000 years and recurrence intervals of the identified palaeoearthquakes in one of the most active faults of the Betic Cordillera.

## 2 GEOLOGICAL SETTING OF THE BAZA FAULT

The normal Baza Fault is located in the Guadix-Baza basin (central Betic Cordillera, fig. 1), in the region where Nubia and Eurasia converge at a rate of approximately 4 to 6 mm/yr (see review by Nocquet, 2012). In this NW-SE convergent geodynamic setting, one of the main tectonic features is the existence of perpendicular tension with a main ENE-WSW orientation of  $\sigma_3$ . This stress setting produces the ENE-WSW extension responsible for highly dipping normal faults since the Miocene (Galindo-Zaldívar et al. 1999).

The Baza fault (fig. 1) is the main active structure of the Guadix-Baza basin and one of the most important active faults of the Betic Cordillera, which accommodates a significant portion of the ENE-WSW extension. This normal fault extends 37 km, with a strike varying from N-S to NW-SE, dipping 45°-65° to the east (Alfaro et al., 2008; García-Tortosa et al., 2011). The width of the fault zone varies from ca. 0.2 km in the north, with one main strand, to ca. 7 km in the south, with more than 13 strands. The total fault throw, from the late Miocene to the present, is ca. 2 km (Alfaro et al., 2008).

Recent fault activity has developed a 30-km-long mountain front. The long-term vertical slip rate ranges between 0.12 and 0.49 mm/year, estimated using a Tortonian stratigraphic marker (Alfaro et al., 2008; Sanz de Galdeano et al., 2012;) and a Middle Pleistocene geomorphological marker (García-Tortosa et al., 2011), respectively. Fernández-Ibáñez et al. (2010) indicate that part of the total throw of the Baza fault could be induced by the isostatic rebound linked to differential erosion. The higher slip rates proposed by these authors (0.49-2.35 mm/year; Fernández-Ibáñez et al., 2010) are inconsistent with other geodetic or geologic fault slip rates of the central Betic Cordillera.

The Baza Fault presents both historical and instrumental associated seismicity, including the 1531 Baza Earthquake (Alfaro et al., 2008), with an assigned intensity of VIII-IX MMI (Martínez Solares and Mezcua, 2002). The assigned macroseismic magnitude  $m_b$  of the 1531 Baza earthquake is 6 (Sanz de Galdeano et al., 2012), i.e., very close to the minimum magnitude threshold of surface rupturing events.

The Baza Fault constitutes a major tectonic structure of the Guadix-Baza basin, and it has influenced the geological, sedimentological, and geomorphological evolution of the basin. The basin presents a highly asymmetric structure, with sediments thickening westward, reaching a maximum observed thickness of ca. 2200 m near the Baza Fault (Haberland et al., 2017). The sedimentary fill of this basin consists of upper Miocene marine rocks and Pliocene/Pleistocene fluvial and lacustrine rocks (Vera, 1970). The marine to continental transition was the consequence of regional uplift of the central Betic Cordillera. The relative uplift of the surrounding relief created differential subsidence, allowing endorheic continental sedimentation in the basin during the Pliocene and most of the Pleistocene (Vera, 1970; Peña, 1985; Gibert et al. 2007). Extensive sedimentation in the Guadix-Baza basin ended when the basin became exorheic in the middle Pleistocene (ca. 500 ka), after a tributary of the Guadalquivir river captured the drainage of the basin towards the Atlantic Ocean. After that, the basin underwent erosive incision and became an alluvial plain that includes some perennial fluvial systems and many ephemeral rivers (fig. 1). However, the inherited low gradient permits local deposition restricted to alluvial fans and piedmont deposits on the basin margin and on fluvial terraces and valley-bottom deposits towards the basin centre. When conditions changed from endorheic to exorheic, the basin presented a flat

geomorphic surface, a glacia, which has been partially preserved and is a useful marker of recent deformation (García-Tortosa et al., 2011).

After the transition of the basin from endorheic to exorheic, the activity of the Baza Fault progressively generated several topographic escarpments along the fault trace. The fault also produced a major mountain front, nearly 30 km long, developed in Plio-Quaternary sediments of the basin infill. This mountain front is not at the contact between the basement rocks and the sediments (see the discussion in Garcia-Tortosa et al., 2008 and 2011), as the active Baza fault zone is developed in recent soft rocks (Pliocene and Quaternary in age).

### 3 METHODOLOGY

After a detailed geomorphic and geological analysis of the entire Baza Fault, we selected six sites for digging trenches. Only two of these sites (Carrizal and Altichuelas, fig. 1) yielded useful palaeoseismological results.

We interpret the data from trenches in terms of surface-rupturing seismic events. This interpretation relies mainly on the geometric relationships existing between sedimentary units and fault strands detected on the trenches' walls.

To date the proposed palaeoseismic events, we used several radiocarbon, optically stimulated luminescence (OSL), and palaeontological samples. Most of the dated samples (Table 1) are charcoal detrital fragments. This represents the main issue of our interpreted rupture history, as the sample age characterises a maximum constraint for the containing unit. We also dated two continental gastropod shell samples (Table 1).

Large terrestrial gastropods are often avoided for  $^{14}\text{C}$  dating because many taxa incorporate “dead” carbon from carbonate rocks when building their shells. This phenomenon, referred to as the “Limestone Problem” (Goodfriend and Stipp, 1983), can cause the radiocarbon ages of gastropod shells to be as much as ca. 3000 yr. too old. Despite this, we included the dated snail samples in our analysis, but instead of the analytical error, we considered an error of 3200 yr. for these samples.

We integrated all the numerical dates in a Bayesian statistics analysis for more-accurate dating. For this purpose, we used OxCal software (Bronk Ramsey, 2009a, 2009b). Our OxCal models use depositional models, not depth-dependent simple sequences (Bronk Ramsey & Lee, 2013). We removed date outliers on the basis of geological judgement, age inconsistencies (e.g., stratigraphically inverted ages), and the Oxcal agreement index (we considered values under 60% as having poor agreement). In building our models, we considered that Oxcal software includes two commands to generate probability density functions (PDFs) for undated events: *Boundary* and *Date*. *Boundary* should be used when the sampling density or deposition type differ within different sections of a sequence (Bronk Ramsey, *written commun.*, 2010). Moreover, we also took into account that the general Oxcal setup is well suited to analysis characterised by numerous, overlapping minimum- and maximum-limiting ages. For earthquakes that do not match these characteristics the most common Oxcal procedure (Lienkaemper and Bronk Ramsey, 2009) may lead to geologically meaningless results. Details of models constructed will be given below, in the sections describing trenches walls and palaeoseismic events.

Event correlation between walls and/or trenches relies on two main criteria: i) our qualitative assessment based on geological judgement and ii) a quantitative calculation of the degree of overlap between probability density functions obtained from the Oxcal models following the methodology proposed by DuRoss et al. (2011) (see below for details). We finally computed recurrence intervals using a Monte Carlo simulation. In all cases, numerical ages are expressed as a range of 95.4% of confidence besides of the mode.

## 4 RESULTS

### 4.1 Carrizal site

The Carrizal site is located in the central part of the Baza Fault (UTM 30S526386/4145217, fig. 1). In this area a fault zone of a 1 km wide including several NNW-SSE striking strands (fig. 1 and 2), is examined. Offsets of the Pleistocene units indicate that most of the Baza Fault cumulative slip concentrates along two main strands (fig. 2). We focused our analysis on the Carrizal sector, where the eastern main strand intersects recent fluvial deposits.

The Carrizal sector is characterised by a vertical sequence of different flat landforms (fig. 2). The highest landform (surface A) is an extensive, flat surface, gently dipping towards the centre of the basin (to the East) corresponding to the glacis of the Guadix-Baza Basin. Erosive incision in this sector developed three gullies running perpendicular to the Baza Fault, which join in the Barranco del Agua creek. The other two flat landforms recognised (surfaces B and C) are related to these gullies. Surface B dips very gently towards the E, and is located at ca. 8-10 m above the present thalweg. This older partially degraded

surface is the top of a fill fluvial terrace, characterised by an alluvial deposit that (formerly) buried the river valley bottom; this alluvial deposit has a highly variable thickness, controlled by fault displacement (see below) and valley morphology. Surface C is located at ca. 1-3 m above the present thalweg. This surface is the floodplain of the channel. The fault strand cropping out in the Carrizal sector is responsible for a ca. 20 m offset of the glacis (surface A, fig. 2). Moreover, this fault strand produces a ca. 2-3 m high fault scarp that separates surface B and the Pleistocene deposits; this fault scarp is not visible in the lower terrace or along the thalweg of the present drainage network.

Carrizal trench was dug on the left side of the Barranco del Agua creek, on surface B and across the fault strand (fig. 2). In the next section, we describe the stratigraphy, structure, and palaeoseismological interpretation observed in the trench.

#### 4.1.1 Trench stratigraphy

Stratigraphic units in this trench are described in detail in Appendix 1. We grouped these units in bedrock units, fluvial terrace deposits, and modern topsoil. In order to constrain the date of the stratigraphic units described below, we collected 27 charcoal samples (Fig. 3) and carried out radiocarbon analyses in 6 of them (fig. 3, Table 1).

The bedrock units exposed in the trench are Pleistocene continental deposits of the Guadix-Baza Basin; these units consist of extensive and well-graded deposits including silts, clays, fine sands, marls, and carbonates. We interpret a modern topsoil developed on the fluvial deposits as a massive, poorly sorted, loose, matrix-supported gravel unit, including abundant plant roots (fig. 3).

Fluvial terrace deposits appear unconformably over the bedrocks units. Surface B corresponds to the top of fluvial terrace deposits. Terrace units are made of poorly sorted gravels, sands, silts, and clays. In the north wall of the trench, four terrace units (T1 to T4, fig. 3) were distinguished; each of these units consists of poorly sorted, matrix supported, fine gravels (maximum clasts size 1 cm). Sources of gravel clasts are Pleistocene bedrock strata. These fine gravels are interbedded with fine sands and silt levels, up to 3 cm thick. Clay levels less than 1 cm thick are also present. In the south wall (fig. 3) the terrace consists of the same poorly sorted, matrix supported fine gravels with thin, fine-grained interbeds. However, in this wall the terrace deposits are much thinner and therefore, together with poor outcrop conditions, we could distinguish only two units in it (TS-lower and TS-upper). Considering the erosive base and the gently northward dip of the terrace, we postulate that unit TS-upper should be the equivalent to one of the uppermost units in the north wall (fig. 3). T3 is also the youngest dated unit in the North wall (CAR-N8, calibrated age of 22582-21993 cal. yr BC). In the south-wall terrace, the only dated sample was collected from unit TS-upper (sample CAR-S4), which yielded a calibrated age of 17643-17167 cal. yr BC. Consequently, we postulate in our analysis that unit TS-upper is probably younger than unit T3 and that it is therefore likely equivalent to unit T4. However, as numerical ages come from detrital charcoal samples (indicating a maximum age for the containing unit), we cannot completely rule out that unit TS-upper in the south wall could be laterally equivalent to a unit lower than T4 in the north wall.

#### 4.1.2 General trench structure



The overall tectonic structure exposed on the trench walls corresponds to a half graben bounded by a main fault strand (F10), and a roll-over fold in the hanging wall (fig. 3). The ca. 7 m width fault zone is highly asymmetric, as the fault core is located in its western end and the damage zone extends only eastwards. The fault core, corresponding to F10, consists of a ca. 5 cm wide cataclastic zone. The damage zone, developed in the bedrock units, consists of a highly sheared zone (F16 to F50) where only remnants of the primary rock structures are preserved. In the non-cohesive bedrock units, rocks are smeared out along the damage zone shear planes. Fault F10 steepening (refraction) lead to a slightly sheared zone in the terrace units. This sheared zone comprises several sub-vertical tension cracks (fig. 3), which we interpret as coseismic refraction of extensional failure as it passes from bedrock to terrace units, probably caused by a lack of confining pressure near the surface and the existence of a true tensional stress field (Mercier et al., 1983; McCalpin, 2009).

Terrace units dip towards the main fault strand observed in the trench wall (see below), but the dip steepens with increasing age and depth. Moreover, terrace units vary in thickness along-section, as units thicken towards the fault and thin in the east part of the trench. Considering these features, we interpret the terrace units as a progressive unconformity, indicating progressive downward tilting towards the fault.

Several filled fissures appear in both the north (Fiss1 to Fiss3) and south walls (Fiss4) (fig. 3). Fiss1 to Fiss3 are related to the above-mentioned sheared zone developed in the terrace units. The big (> 1 m wide) fissure Fiss4 of the south wall (fig. 3) is filled with unconsolidated, clasts supported breccias organised in thick beds. These beds present a concave morphology that we interpret as the result of upward dragging related to

differential compaction. Fissure 4 present a different geometry respect the rest of fissures observed in the trench walls, as it is bigger. We postulate that this different geometry is because of fissure 4 opens in the hangingwall of the main deformation zone, consisting of much more firm rocks (consolidated carbonates and marls). As no fault can be discerned at the base of this fissure, we interpret it as a tension crack.

#### 4.1.3 Surface rupturing history of Carrizal trench

In this section, we present the main palaeoseismic features of both walls of Carrizal trench and their interpretation in terms of surface rupturing palaeoseismic events. Moreover, we also discuss the dating of events based on the Bayesian statistical analysis performed. This trench contains evidence for five to seven fault rupture events (events Car\_e1 to Car\_e7, fig. 3). Most of the dated samples (fig. 3, Table 1) are charcoal detrital fragments. In addition, two large (maximum dimension ca. 4 cm) continental gastropod shells samples were collected from Fiss4 unit; rather than charcoal, gastropods shells are considered as *in situ* samples, because of good preservation conditions. As mentioned above, we included the dated snail samples in our analysis; but, to account for the “dead” carbon issue, we considered an error of 3200 yr. for this sample.

Data from all these samples were introduced in an Oxcal model to analyse the ages of events (Appendix 1). We built a composite model including data from both walls (north and south). Samples CAR-N2 and CAR-N12 were removed from the model after initial consideration, as they were considered as outliers.

Event Car\_e1

The oldest event (Car\_e1) is represented by ruptured of faults F16, F18, F20, F30, and F40, that intersect bedrock units and are capped by the terrace (fig. 3). According to this, Car\_e1 should be older than the terrace deposition.

We modelled in Oxcal the age of event Car\_e1 as a *Boundary* (Appendix 1), because of the different deposition type below and above the event. This event has a minimum age limited by detrital charcoal from unit T1 (sample CARN-4), but its maximum age is limited by the palaeontological date from the bedrock units (Agustí et al., 2001). We infer that the minimum age from the terrace unit is a better approximation of the event time than the maximum-limiting age from the bedrock sediments because the terrace was likely deposited because of rupture-related generation of the necessary accommodation space. To account for this inference, we paired the event *Boundary* in the Oxcal model with a separate *Zero Boundary* command representing the time lapse between the limiting ages (as proposed by DuRoss et al., 2011). With all these constraints, the Oxcal model yielded an age for event Car\_e1 between 45378 and 33205 cal. yr BC (Fig. 3, Appendix 1).

#### Events Car\_e2 to Car\_e4

Events Car\_e2 to Car\_e4 are deduced from the stratigraphic architecture of the terrace units. As previously described, the four terrace units recognised in the south wall (T1 to t4, fig. 3) present a progressive unconformity indicating progressive tilting down towards the fault. We interpret this geometry as the result of progressive back-tilting related to repeated faulting during four successive palaeoseismic events (Car\_e2 to Car\_e4). We assume that the upper boundaries of the fine-grained thin beds were initially horizontal. Because these beds are sub-parallel to fine gravels, these latter are

also assumed to have been horizontal, whereas the lower boundaries of the units may have had some gentle dips. Therefore, we postulate that after event Car\_e1, a half graben resulted from the westward tilting of the bedrock units. Afterwards, the deposition of unit T1 occurred. At the end of this deposition, the bedding was horizontal. A successive faulting event (Car\_e2) tilted unit T1. This event could also have been responsible for the opening of fissure Fiss1, which only deforms up to unit T1. However, because the upper tip line of this fissure cannot be discerned (being obscured by fissure Fiss2), we cannot rule out that fissure 1 was developed in a later fracturing episode. Event Car\_e2 was followed by the deposition of unit T2.

According to the above, Car\_e2 should be younger than unit T1 (sample CAR-N4 predating) and older than unit T2 (sample CAR-N17 postdating). We found a modelled age for event Car\_e2 of 33465 and 24347 cal. yr BC.

Evidence for the next palaeoseismic event (Car\_e3) is equivalent to pieces of evidence previously discussed for event Car\_e2 (i.e., horizontal deposition of unit T2 and successive faulting tilting, fig. 3). The age of event Car\_e3 is constrained between units T2 and T3 (sample CAR-N17 predating and sample CAR-N8 postdating). In this case, we determined a modelled age of 24229 and 22241 cal. yr BC.

Again, we interpret the tilting of the top of unit T3 top (assumed initially horizontal, fig. 3) as a younger palaeoseismic event (Car\_e4). This new event is also indicated by the rupturing of units T1 and T2 by fissure Fiss2 (deforming up to unit T3). The age of event Car\_e4 is constrained by the deposition of unit T3 (sample CAR-N8 predating) and of unit T4 (sample CAR-N12 postdating). Assuming the correlation of walls previously discussed, the south wall unit TS-upper also constrains event Car\_e4 (sample CAR-S4

postdating). The Oxcal model yielded an age for event Car\_e4 of 22223 and 17538 cal. yr BC.

#### Event Car\_e5

In our preferred palaeoseismic interpretation of the Carrizal trench, the youngest event recorded in this wall (Car\_e5) was responsible for the deformation of unit T4, TS-upper, and the opening of fissure Fiss3, but it caused no identifiable tilting of the units (probably obscured by later development of the present topsoil, fig. 3). The large fissure located in the eastern part of the south wall (fissure Fiss4) does not intersect the terrace units; however, a radiocarbon date is available from the base of the fissure infill, as sample CAR-Sc2 yielded an age of 767-492 cal. yr BC (unmodeled age; fig. 3, table I). We use this age (post-dating fissure opening) to integrate the fissure in the rupture history of the trench. We postulate that fissure Fiss4 was immediately filled after the fissure was opened (i.e., the fissure did not remain open and was void for tens of thousands of years). Consequently, the event responsible for fissure Fiss4 should be older than 767-492 cal. yr BC. Nevertheless, this date could be younger, as sample CAR-Sc2 is a fossil shell of a large terrestrial gastropod that can yield ages ca. 3000 yr too old. As previously discussed, event Car\_e4 took place a long time before (between 22223 and 17538 cal. yr BC). Consequently, we postulate that fissure Fiss4 opened during an event younger than event Car\_e4. Because we are discussing in this section a minimum number of events hypothesis, we assume that this younger event responsible for the opening of fissure Fiss4 was the same event that caused the deformation of unit T4 and TS-upper and the opening of fissure Fiss3, i.e., event Car\_e5 (the youngest event recorded).

Accordingly, event Car\_e5 is predated by units T4 and TS-upper (sample CAR-S4) and is postdated by fissure Fiss4 infill and the topsoil (samples CAR-Sc2, CAR-N10, and CAR-N15). To incorporate the previously mentioned time offset related to the age of the terrestrial gastropod into the radiocarbon timescale, we inserted a *Delta\_R* command into our Oxcal model, assuming an uncertainty of 3200 yr. With these constraints, the Oxcal modelling gave an age of 17123 and 760 cal. yr BC for event Car\_e5.

#### Event Car\_e6

An alternative scenario involving a maximum number of events can be postulated for the last part of the rupturing history recorded at Carrizal trench. Radiocarbon ages of samples from the units post-dating event Car\_e5 and modelled ages determined from the Bayesian analysis seem to suggest that the event responsible for the deformation of units T4 and TS-upper and the opening of fissure 3 (event Car\_e5) is considerably older than the deposition of the fissure Fiss4 infill (fig. 3, table I). We postulated that the fissure infilling should have started immediately after crack opening and not a few thousand years later; consequently, the different ages determined between Car\_e5 and the base of fissure Fiss4 infill could indicate that the fissure was generated during a different event. If this is correct, an extra event should be added to the previously discussed rupture history. The addition of this extra event (event Car\_e6) to our Oxcal model shifts the age of event Car\_e5 to 17546-4163 cal. yr BC. For event Car\_e6, the model yielded an age of 13809 and 558 cal. yr BC. The ages of the other of events (events Car\_e1 to Car\_e4) undergo minor changes (fig. 3).

#### The 1531 Baza Earthquake

According to our models, the youngest event registered in the Carrizal trench occurred between 17123 and 760 cal. yr BC (minimum-number-of-events hypothesis) or between 13809 and 558 cal. yr BC (maximum-number-of-events hypothesis). These ages imply that the 1531 Baza earthquake was not recorded in the Carrizal trench, as sedimentation in the terrace ended a long time before 1531 AD (the younger dated sample in the terrace yielded an age of 22582-21993 cal. yr BC).

In summary, data from the Carrizal trench account for a minimum of 5 surface-rupturing events in the Baza Fault during the last ca. 23000 yr (our preferred interpretation). An extra event should be added to this number if we assume that fissure 4 was the consequence of a different event. These data also indicate that the 1531 AD Baza Earthquake was not recorded in the Carrizal trench.

#### 4.1.4. Single event displacement in the Carrizal Trench

Poor outcrop conditions in the Carrizal Trench area hampers an estimation of single event displacement (SED) by restoring the tilting of the angular unconformity of the Carrizal trench. In addition, no stratigraphic marker can be traced both in the hangingwall and in the footwall of the main fault strand, consequently the total throw related to this strand cannot be estimated either. However, the presence of the top of the basement in the hangingwall permit a calculation of the minimum offset produced by the main fault strand (F10, fig. 3). We calculated a minimum throw of  $2.5 \pm 0.1$  m for the N wall and of  $1.4 \pm 0.1$  m for the S wall. By dividing this minimum throw by the number of events postulated above we obtained a minimum SED of  $0.4 \pm 0.1$  m for the minimum number of events scenario and of  $0.3 \pm 0.2$  m for the maximum number of events scenario.

## 4.2 Altichuelas site

The Altichuelas site is located 2.5 km NE of Caniles village, in the southern part of the Baza Fault (UTM 30S526386/4145217, fig. 1). In this sector, the 7-km-wide fault zone splits into several NW-SE-slipping fault strands (fig. 1). We focused our analysis on this area because one of the fault strands offsets recent alluvial deposits.

In the Altichuelas sector, the Rambla de Valcabra ephemeral river flows from South to North (fig. 4), sub-parallel to the fault zone. This river is dry for long periods of time and only experience flow after there has been sufficient rain in the catchment area. The Rambla de Valcabra gully, like many others in the Guadix-Baza Basin, can be described as a bedload river (Nichols, 2009), i.e., a river with a high proportion of sediment carried out along the channel floor.

In the Altichuelas sector (fig. 4), two flat geomorphological surfaces related to the Rambla de Valcabra gully appear, a higher surface located at ca. 15 m above the present thalweg and a lower surface at ca. 1 m. We interpret the upper surface as a fill fluvial terrace. The lower terrace represents the presently active floodplain of the Rambla de Valcabra gully. In this sector, the channel bends towards the East; consequently, the river channel is intercepted by one of the Baza Fault strands. The Altichuelas trench was excavated in an area where the fluvial terrace is offset by the fault strand.

### 4.2.1 Trench stratigraphy

To constrain the date of the stratigraphic units described below, we collected 8 charcoal and 11 sand samples (Fig. 5), and performed radiocarbon analyses in 2 charcoal fragments and OSL analyses in 7 sand samples (fig. 5, Table 1). We grouped the units of this trench into bedrock units, point-bar deposits, channel deposits, and modern topsoil.



The trench bedrock units (Fig. 5) are Pleistocene well-bedded and well-sorted deposits including silts, clays, fine sands, and gravels; we interpret these units as fluvial floodplain deposits.

Above the bedrock units, a slightly bedded, matrix-supported gravel unit appears (unit A, Fig. 5). We interpret that this unit could be a channel-related deposit, perhaps an alluvial terrace. In the north wall, we distinguished four sub-units within unit A (units A1 to A3). Units A1 and A3 consist of slightly bedded, poorly sorted, matrix-supported gravel with bedrock-derived angular clasts. In unit A2, the bedding is clearer. Two samples constrain the age of these units (Fig. 5, Table I): unit A1 is dated by sample ALT-N12 (14177-13797 cal. yr BC), while unit A3 is dated by ALT-N61 (8385-7185 cal. yr BC). In the south wall, no subunits could be distinguished within unit A because of poor outcrop conditions. However, the available numerical age (sample ALTS-8, 9113-8630 cal. yr BC) lead us to propose that unit A in the South wall is probably equivalent to one of the uppermost subunits in the North wall (A2 or A3).

Unit CW was deposited above unit A1 and is topped by unit A2. Unit CW presents a wedge shape (thickest at the fault and thinning away from the fault) and consists of clast-supported, massive, very poorly sorted gravels. The clasts in this unit are highly angular and mainly consist of fragments of bedrock units. We interpret unit CW as a scarp-derived colluvial wedge.

Unit B unconformably overlies both unit A and bedrock units (Fig. 5). We divided unit B into several sub-units consisting of channel-shaped bodies with erosive basal contacts and fining upwards sequences. These sequences include a basal clast-supported gravel lag followed by slightly bedded sands, silts, and fine gravels. We interpret unit B as a

fluvial channel deposit. Unit B is dated by samples ALT-S50 (955-1175 cal. yr AD), ALT-S53 (865-1125 cal. yr AD), and ALT-N60 (1115-1315 cal. yr AD). Finally, a poorly sorted, loose gravelly unit including abundant plants roots is interpreted as modern topsoil (Fig. 5).

#### 4.2.2 General trench structure

The fault zone exposed in the trench walls (Fig. 5) consists of a ca. 5-m-wide highly sheared zone including several fault strands (F01 to F30). In this sheared zone, only remnants of the primary rock structures are preserved in the bedrock units. These bedrock units describe a roll-over fold East of fault F05. In contrast, these units have been tilted up by drag on fault strand F30, as has unit B4 East of fault strand F05 (south wall). Several imbricate reverse faults appear in the north wall in unit A (F25). These reverse separations could be the consequence of the combination of faulting on a sloping ground surface and the tendency for faults to steepen toward the ground surface (e.g., Berryman et al., 2008). Several filled fissures appear in both the north and south walls (fig. 5).

#### 4.2.3 Surface rupturing history of the Altichuelas trench

In this trench, the correlation of palaeoseismic features between walls is not so clear (see below). Therefore, we propose a separate surface rupturing history for each wall (north and south). Next, we correlate the two walls to propose a composite history for the entire trench.

##### 4.2.3.1 Altichuelas trench south wall

The south wall contains evidence of 3 surface rupture events (events AltS\_e1 to AltS\_e3, fig. 5). To constrain the date of the seismic events described below, we collected 8 charcoal samples (fig. 5) and carried out radiocarbon analyses in one of them (fig. 5, Table 1). All these samples are charcoal detrital fragments, indicating a maximum constraint for the containing unit, as discussed above. We also collected 7 OSL samples and analysed 5 of them. The data from all these samples were entered in an Oxcal model to evaluate the ages of the events (Appendix 1). OSL dates were introduced in the model as *C\_Dates*, which returns a PDF for calendar dates with normally distributed errors.

We describe in the next paragraphs the main palaeoseismological evidence for these events, together with the details of the constructed Oxcal models. Event ages are discussed below.

#### Event AltS\_e1

The oldest event (AltS\_e1) is represented by the rupture of faults F10, F20, and F30, which intersect bedrock units and are capped by unit A (Fig. 5a). AltS\_e1 should be younger than the bedrock units (sample ALT-N03 predating) and older than unit A (sample ALT-S08 postdating). We modelled this event in Oxcal by introducing a *Boundary* command because of different deposition types between the constraining units (Appendix 1).

#### Event AltS\_e2

The next Palaeoseismic event recorded in this wall (AltS\_e2) is expressed by the faulting of unit A and by several fissures observed in the upper-central part of the trench (fissures Fiss1 to Fiss4, Fig. 5a). The above-mentioned fissures developed in unit A and are capped by unit B4. We postulate that these fissures appeared because of forward-tilting related to faulting, probably along fault F05. Therefore, AltS\_e2 should be older than unit A

(predating sample ALT-S08) and younger than unit B4 (postdating sample ALT\_S53, Appendix 1).

#### Events AltS\_e3 and AltS\_e4

The youngest event in this south wall (AltS\_e3) is recorded by the deformation of unit B4, tilted up by drag on fault strand F05 (Fig. 5a). This drag folding is clearly expressed at the base of unit B4. At the top of this unit, drag folding is not so clear, because of poor outcrop conditions (we cannot completely rule out that the upper part of unit B4 actually post-dated event AltS\_e3).

This event is younger than the lower part of unit B4 (whose age is constrained by sample ALT-S53, 865-1125 AD, unmodeled age), but no direct upper constraint is available. To further constrain event AltS\_e3, we also considered the Spanish Earthquake Catalogue (IGN, 2017). According to a recent study by the Spanish National Geographical Institute (Martinez-Solares et al., 2013), this catalogue can be considered complete in our study area from 1520 AD onward for earthquakes with an assigned macroseismic magnitude higher than 5.5-5.9 Mw. Therefore, we added a *C\_Date* command to our Oxcal model to account for this constraint (Appendix 1).

As indicated above, the assigned macroseismic magnitude mb of the 1531 AD Baza earthquake is 6.0 (Sanz de Galdeano et al., 2012), implying that this event may or may not have caused surface rupturing. Consequently, we postulate three hypotheses (Fig. 5c) and constructed three different Oxcal models. The first two hypotheses (H1S and H2S) imply that the Baza Earthquake produced surface rupturing. i) The first hypothesis (HS1) assumes that event AltS\_e3 corresponds to the Baza Earthquake (i.e., Baza Earthquake is recorded by faulting of the base of unit B4). In this case, its age should be

1531 AD. ii) The second hypothesis (HS2) postulates that event AltS\_e3 does not correspond to the Baza Earthquake (i.e., Baza Earthquake produced surface rupture but it was not recorded in the trench because rupture propagated along a different fault strand or because of the incompleteness of the Palaeoseismological record). In that case, event AltS\_e3 should be younger than deposition of unit B4 and older than 1520 AD (earthquake catalogue constrain), so we added to the Oxcal model (Appendix 1) a *Date* command (corresponding to AltS\_e3) and a *Boundary* command (corresponding to 1531 AD Baza Earthquake). In these first two hypotheses, the 1531 Baza Earthquake was modelled in Oxcal by introducing a *Boundary* command (Appendix 1). iii) The third hypothesis (HS3) implies that the Baza Earthquake did not produce surface rupturing (we postulate that Baza Earthquake occurred along the Baza Fault but at depth). So AltS\_e3 correspond to an event younger than deposit of unit B4 and older than Baza Earthquake and 1520 AD (earthquake catalogue constrain). In this case, no further constraints were added to the Oxcal model; i.e, most recent age is the present (Appendix 1).

#### Events ages

Our observations point to a surface rupturing history for this south wall spanning three events for the last ca. 16000 years. However, the modelled ages of these events vary depending on the hypothesis considered (Fig. 5a and 5c), i.e, depending on whether we assume that the Baza Earthquake produced surface rupture and whether it was recorded in the trench. The modelled ages of hypotheses HS2 and HS3 are very similar, the main difference being that HS2 involves one extra event (Baza Earthquake) not recorded in the trench. In HS1, the modelled ages of events AltS\_e1 and AltS\_e2 present

minor differences from the other two hypotheses. The main difference is the age of event AltS\_e3, which this hypothesis assumes to be 1531 AD.

#### 4.2.3.2 Altichuelas trench north wall

The north wall offers evidence of three surface rupture events (events AltN\_e1 to AltN\_e3, fig. 5b). To constrain the date of the seismic events described below, we collected and dated one detrital charcoal sample (fig. 5b, Table 1). We also collected 3 OSL samples and analysed 2 of them (fig. 5b, Table 1).

Again, data from all these samples were introduced in Oxcal to model the ages of the events (Appendix 1). We describe in the next paragraphs the main palaeoseismological evidence for these events, together with the details of the Oxcal models constructed. Event ages are discussed below.

##### Event AltN\_e1

The oldest event (AltN\_e1) is represented by the rupture of faults F15 and F17, which intersect bedrock units and are capped by unit A1 (Fig. 5b). Accordingly, AltN\_e1 should be younger than the bedrock units (predating sample ALT-N03) and older than the deposition of unit A1 (postdating sample ALT-N12).

##### Event AltN\_e2

The next palaeoseismic event registered in the north wall of the Altichuelas trench (AltN\_e2) was responsible for the offset of unit A1 by fault strand F01 and the subsequent deposit of the colluvial wedge CW (Fig. 5b). Consequently, event AltN\_e2 should be younger than unit A1 (sample ALT-N12 predating), and older than the units that cap Fault F01, i.e., units A2 and A3 (whose age is constrained by sample ALT-N61).

## Event AltN\_e3

The next Palaeoseismic event deduced in this wall (AltN\_e3, Fig. 5b) is indicated by offset along fault strands F05, F06, F04, and F03. However, the structural relations are not evident between the examined faults and unit A3. Only the base of unit A3 is undoubtedly offset by fault strand F05 and minor strands F06, F04, and F03, but the trace of the faults is not so clear within this unit. Moreover, no evident clasts parallel to the strands appear in unit A3, and the material at the contact seems to be similar in hardness to material far from the contact. Only a fissure related to F06 is visible. However, in the south wall, F05 displaces units A and B (fig. 5a), so we assume that in this north wall, F05 also ruptures the entire unit A, as do strands F06, F04, and F03.

The stratigraphic correlation between walls indicates that the offset along F05 took place after deposition of unit B (dated by sample ALTN-60). Thus, we assume that this latter unit represents the lower constraint for the event AltN\_e3. As mentioned above, it is unclear whether the 1531 AD Baza earthquake caused surface rupturing. Consequently, we again postulated three hypotheses (Fig. 5c) and constructed three alternative Oxcal models (Appendix 1) analogous to the one discussed for the south wall. Again, the first two hypotheses (H1N and H2NS) imply that the Baza Earthquake produced surface rupturing (modelled in Oxcal as a *C\_Date* command, Appendix 1). i) In the H1N hypothesis, event AltN\_e3 corresponds to the Baza Earthquake, and in this case, its age should be 1531 AD. ii) In hypothesis H2N, event AltN\_e3 does not correspond to the Baza Earthquake (i.e., Baza Earthquake produced surface rupture along somewhere else along the Baza Fault, so it was not recorded in the trench). iii) The

third hypothesis (HN3) implies that the Baza Earthquake occurred in depth along the Baza Fault but it did not produce surface rupturing.

#### Events ages

Consequently, our observations point to a surface rupturing history for this north wall spanning three events for the last ca. 16000 years. However, as discussed above, the modelled ages of these events vary depending on the hypothesis considered (Fig. 5b and 5c). The modelled ages of hypotheses HN2 and HN3 are analogous; the only significant difference is that HN2 invokes one extra fault-scale event (Baza Earthquake) not recorded in the trench. In HN1, the modelled ages of the two older events present minor differences with respect to the same events in the other two hypotheses. The main difference is the age of event AltS\_e3, which this hypothesis assumes is 1531 AD.

#### 4.2.3.3 Composite surface rupturing history of the Altichuelas trench

To propose a composite surface rupturing history of the Altichuelas trench, including observations from both walls, we used (1) a qualitative assessment based on geologic criteria (the key stratigraphic and structural features) together with (2) a quantitative calculation of the overlap of event ages determined after Oxcal modelling. Above, we postulated several hypotheses for the two walls involving different numbers of events (hypotheses HS1 to HS3 and HN1 to HN3). To propose a composite surface rupturing history of the Altichuelas trench accounting for these hypotheses, we considered three scenarios (Fig. 6a): i) The first scenario involves surface rupture during the 1531 AD Baza Earthquake. This first scenario also assumes that the Baza Earthquake corresponds to the youngest events recorded in both trench walls (AltS\_e3 and AltN\_e3). Therefore, the first scenario involves hypotheses HS1 and HN1 (Fig. 5c, 6a and 6b). ii) The second



scenario also involves that surface rupture during the 1531 AD Baza Earthquake occurred along a different fault strand of the Baza Fault. Consequently, this earthquake does not correspond to the youngest events recorded in the two walls. Consequently, the second scenario involves hypotheses HS2 and HN2 (Fig. 5c, 6a and 6c). This second scenario also implies that other than the three events recorded in the trench, an extra earthquake should be added to the fault surface rupturing history (Baza Earthquake). iii) The third scenario assumes that no surface rupturing occurred during the 1531 AD earthquake. Hence, this third scenario involves hypotheses HS3 and HN3 (Fig. 5c, 6a and 6d).

We discuss in the following paragraphs the event combinations of all three scenarios.

#### *Scenario 1*

The first scenario assumes that the Baza Earthquake produced surface rupture and that it was recorded in the trench.

#### *Events Alt\_e1 and Alt\_e2*

In the first scenario, the modelled age of the oldest event registered in the south wall (AltS\_e1) overlaps with two events registered in the north wall: events AltN\_e1 and AltN\_e2 (Fig. 6b). To determine which event from the north wall better correlates with event AltS\_e1, we calculated the degree of overlap between the site PDFs determined from the Oxcal models for each wall. For this purpose, we followed the methodology proposed by Biasi and Weldon (2009). That is, we combined evidence of ground rupture from individual walls into a pool of all possible composite *ruptures* (a *rupture* is considered a composite event including evidence from several walls; Biasi and Weldon, 2009). Next, we measured the overlap area of each composite rupture to quantify the

quality of the correlation (Biasi and Weldon, 2009; DuRoss et al., 2011). The PDF overlap of a pair of events was computed as the sum of probabilities of each event per 5 yr time bin in the area of overlap. Then, the overlap area measured for composite *ruptures* was computed as the mean overlap area among contributing individual dates in the rupture. For the overlap area to be uniquely determined, events are first ordered by mean date, and pairs are formed successively. Missed events contribute to the number of sites but not the overlap area. In our case, the calculation was quite simple, as there were only two walls and only two possible correlations were involved: AltS\_e1=AltN\_e1 or AltS\_e1=AltN\_e2.

The computed overlaps indicated that AltS\_e1 better correlated with AltN\_e2 (overlap of 0.76) than with AltN\_e1 (overlap of 0.11). Therefore, we postulated that event AltN\_e1 represents the oldest event of the trench (Alt\_e1, 16182-13863 BC), while AltS\_e1 and AltN\_e2 represents the same event, Alt\_e2. This agrees with the geological criteria observed in the trench: event AltS\_e1 is indicated by offset produced by faults F10, F20, and F30, which intersect bedrock units and are capped by unit A (Fig. 5a). We postulated that unit A in the south wall corresponds to unit A2 or A3 in the north wall, and consequently, event AltS\_e1 should be equivalent to event AltN\_e2 (capped by colluvial wedge CW and the subsequent deposition of units A2 and A3, Fig. 5b). To constrain the age of event Alt\_e2, integrating the data from both walls, we combined the separate Oxcal PDFs to generate a single combined PDF (Fig. 6b), following the methodology proposed by DuRoss et al. (2011). For this purpose, we first scaled the trench PDFs, where for each PDF, the sum of the probabilities into a single PDF equals 1. Afterwards, we combined the probabilities into a single PDF by multiplying the probabilities of each wall PDF for each 5 year interval. The resulting combined PDF was

also normalised so that its sum equalled 1. Subsequently, we calculated the event times, reported as a range of 95.4%. After this calculation, we determined that event Alt\_e2 took place between 13725 and 8825 BC.

#### *Event Alt\_e3*

The PDF of the next-youngest event recognised in the south wall (AltS\_e2) overlaps with event AltN\_e2 from the north wall. However, AltN\_e2 better correlates with AltS\_e1 (overlap of 0.76, as indicated above) than with AltS\_e2 (overlap of 0.14) (Fig. 6b). Therefore, we propose that AltS\_e2 represents a new palaeoseismic event, Alt\_e3 (8665 BC-687 AD).

#### *Event Alt\_e4*

The next-youngest event recorded in the south wall (AltS\_e3) caused the deformation of unit B by fault strand F05 (Fig. 5a), and we previously discussed that it could be geologically correlated with event AltN\_e3 in the north wall (deforming unit A3, Fig. 5b). In this first scenario, we assume that both AltS\_e3 and AltN\_e3 represent the Baza Earthquake. Consequently, the age of the composite event Alt\_e4 is 1531 AD (Fig. 6b).

#### *Scenario 2*

The second scenario assumes that the Baza Earthquake produced surface rupture, but it was not recorded in the trench.

#### *Events Alt\_e1 and Alt\_e2*

In the second scenario, the modelled age of the oldest event registered in the south wall (AltS\_e1) overlaps with two events registered in the north wall: events AltN\_e1 and AltN\_e2 (Fig. 6c). Again, the computed overlaps indicated that AltS\_e1 better correlated with AltN\_e2 (overlap of 0.72) than with AltN\_e1 (overlap of 0.08). Therefore, we postulated that event AltN\_e1 represents the oldest event of the trench (Alt\_e1, 16130-13859 BC), while AltS\_e1 and AltN\_e2 represent the same event, Alt\_e2 (13670-8815 BC).

#### *Events Alt\_e3 and Alt\_e4*

The PDF of the next-youngest event recognised in the south wall (AltS\_e2) overlaps with events AltN\_e2 and AltN\_e3 of the north wall (Fig. 6c). The overlap between AltS\_e2 and AltN\_e2 is lower than that between AltS\_e1 and AltN\_e2 (0.72 and 0.14, respectively). Consequently, as discussed above, we include event AltN\_e2 in Alt\_e2 together with AltS\_e1. AltS\_e2 also overlaps with event AltS\_e3 (Fig. 6c). However, the computed overlaps indicate that AltN\_e3 is better correlated with AltS\_e3 (overlap of 0.75) than with AltN\_e2 (overlap of 0.001). Therefore, we propose that event AltS\_e2 represents palaeoseismic event Alt\_e3 (8654 BC-698 AD). Event Alt\_e4 encompasses both AltS\_e3 and AltN\_e3, yielding a composite age of 1130-1505 AD.

#### *Scenario 3*

The third scenario assumes that the Baza Earthquake occurred along the BAza Fault but it did not produce surface rupture.

#### *Events Alt\_e1 and Alt\_e2*

In the third scenario, the modelled age of the oldest event registered in the south wall (AltS\_e1) overlaps again with two events registered in the north wall: AltN\_e1 and AltN\_e2 (Fig. 6d). Again, the computed overlaps indicated that AltS\_e1 better correlated with AltN\_e2 (overlap of 0.72) than with AltN\_e1 (overlap of 0.08). Therefore, we postulated that event AltN\_e1 represents the oldest event of the trench (Alt\_e1, 16067-13775 BC), while AltS\_e1 and AltN\_e2 represent the same event, Alt\_e2 (13670-8815 BC).

#### *Events Alt\_e3 and Alt\_e4*

The PDF of the next-youngest event recognised in the south wall (AltS\_e2) overlaps with events AltN\_e2 and AltN\_e3 of the north wall (Fig. 6d). The overlap between AltS\_e2 and AltN\_e2 is lower than that between AltS\_e1 and AltN\_e2 (0.72 and 0.08, respectively). Therefore, we include event AltN\_e2 in Alt\_e2 together with AltS\_e1, as previously discussed. The overlap of AltS\_e2 with event AltS\_e3 is lower than the overlap between AltS\_e3 and AltN\_e3 (0.002 and 0.75, respectively) (Fig. 6c). Consequently, we propose that event AltS\_e2 represents palaeoseismic event Alt\_e3 (8657 BC-682 AD). Event Alt\_e4 encompasses both AltS\_e3 and AltN\_e3, yielding a composite age of 1125-1510 AD.

#### 4.2.4. Single event displacement in the Altichuelas Trench

Similarly to that above discussed for the Carrizal Trench, the top of the basement in the hangingwall of the main fault strand (F05, fig. 5) indicates a minimum throw for this fault strand of  $3.5 \pm 0.9$  m for the N wall and of  $3.2 \pm 0.8$  m for the S wall. By dividing this minimum throw by the number of events postulated above we obtained a minimum SED

of  $0.8 \pm 0.1$  m. This minimum SED is the same for all the three scenarios discussed, as the all three involve the same number of events (4).

## 5 Earthquake chronologies of the Baza Fault

We integrated the above-discussed results of our palaeoseismic research into an earthquake chronology of the Baza Fault by correlating the resulting PDFs for the Carrizal and Altichuelas sites, following the same procedure discussed above. This correlation is based on the quantitative calculation of the overlap of the event ages obtained from the Oxcal modelling described above. In correlating the site PDFs, we assumed that the Baza Fault is not divided into segments and is prone to large, generally fault-wide, characteristic earthquakes. That is, we interpreted the partial surface rupturing histories at the two study sites and the PDF overlap as evidence of 8 to 10 earthquakes (EQ1 TO EQ10) since ca. 45000 yr BC that ruptured all or most of the length of the Baza Fault. This rationale of using characteristic behaviour is supported by the observation that the fault is defined by prominent structural boundaries and that no segmentation of the fault have been reported. A fault-wide rupture of the Baza Fault (ca. 33 km long) should involve a  $M_w=6.7 \pm 0.34$  or  $7.1 \pm 0.30$  event (according to the empirical relations proposed by Wells and Coppersmith, 1994 and Stirling et al., 2002, respectively). These values are in good accordance with the estimated maximum proposed for the 1531 AD Baza Earthquake ( $m_b=6.0 \pm 0.6$ , Sanz de Galdeano et al., 2012). Values of minimum SED calculated above further support the assumption of a characteristic behavior of the Baza Fault. We consider a maximum rupture length of the Baza Fault ranging between 33 and 37 km (Alfaro et al., 2008). With these data, we obtained an average per-event displacement (AD) of  $0.78-0.90 \pm 0.37$  m and a maximum per-event displacement (MD)

of  $2.06\text{--}2.44 \pm 0.41$  m by using the Wells and Coppersmith (1994) regressions. The regression proposed by Stirling et al. (2002) yielded an AD of  $2.15\text{--}2.20 \pm 0.24$  m. These values are compatible with the minimum SED calculated from our palaeoseismological analysis, ranging between  $0.3 \pm 0.2$  m and  $0.8 \pm 0.1$  m. However, we cannot completely rule out a potential non-characteristic behaviour of the fault, as a rupture involving just half of the fault length could be capable of causing a surface rupture (*sensu* Stirling et al., 2013).

At the Carrizal site, we recorded 5-6 events between 45378 and 558 cal. yr. BC (Fig. 3), while we proposed that 4 events at the Altichuelas site occurred between 16239 cal. yr. BC and 1531 AD (Fig. 6). However, because of the geological uncertainties observed in our trenches, we proposed six different scenarios (i.e., earthquake chronologies) involving different event ages (Fig. 7). These six alternative chronologies (Fig. 7a) correspond to all the combinations between the two scenarios discussed for the Carrizal trench (minimum and maximum number of event scenarios) and the three scenarios of the Altichuelas trench (scenarios 1 to 3).

An initial visual analysis of the overlap of events for all the proposed chronologies (Fig. 7c-7h) indicates that only the youngest events from the Carrizal trench overlap with the Altichuelas surface rupturing history. This implies that the two study sites record different parts of the Baza Fault earthquake chronology: the younger part is better recorded at the Altichuelas site, while the older part is better recorded at the Carrizal site. In addition, because the four older events recorded in the Carrizal trench are common for both trench scenarios (Fig. 3 and 7), the four older fault-wide earthquakes

(EQ1 to EQ4) are also common for all the earthquake chronologies we propose for the Baza Fault (Fig. 7).

As the younger part of the Baza Fault earthquake chronology is recorded in both trenches (see below) we postulate that all the surface-rupturing events are fault-wide earthquakes. However, as the Altichuelas trench does not record the older part of the Baza Fault earthquake chronology (i.e., no events older than 16182 AD are deduced in this trench), we cannot completely rule out that the four older events are not fault-wide earthquakes.

### 5.1 Earthquake chronology 1

Earthquake chronology 1 encompasses the minimum-number-of-events scenario from the Carrizal trench and Scenario 1 from the Altichuelas trench (Fig. 7a).

The overlap analysis of the modelled PDFs (Fig. 7c) indicates that the four oldest events recorded at the Carrizal site (Car\_e1 to Car\_e4) do not overlap with any of the event PDFs from the Altichuelas site, as mentioned above. Therefore, we propose that these four events represent four fault-wide earthquakes (Fig. 7c): EQ1 (45378-33205 BC), EQ 2(33465-24347 BC), EQ 3 (24229-22241 BC), and EQ4 (22223-17538 BC).

The youngest event recorded at the Carrizal site (Car\_e5) partially overlaps with the three older events from the Altichuelas site (Alt\_e1, Alt\_e2 and Alt\_e3) (Fig 7c). We assume that event Car\_e5 actually correlates with one of the two older events from the Altichuelas site because of the high computed degree of overlap between two of these events (see below). To determine which event from the Altichuelas site event Car\_e5 best correlates with, we calculated the degree of overlap between the site PDFs obtained from the Oxcal models for each trench. For this purpose, we again followed



the methodology proposed by Biasi and Weldon (2009). The analysis of the PDF overlap indicates that the *rupture* Car\_e5=Alt\_e3 presents a greater overlap than *ruptures* Car\_e5=Alt\_e1 and Car\_e5=Alt\_e2 (0.49 vs. 0.18 and 0.32, respectively). Hence, we postulate that event Alt\_e1 represents fault-wide earthquake EQ5 (15705-13925 BC), Alt\_e2 represents EQ6 (13725-8825 BC), and earthquake EQ7 encompasses events Car\_e5 and Alt\_e3. To constrain the age of earthquake EQ7, integrating the data from Car\_e5 and Alt\_e3 events into a single composite PDF, we followed the same procedure discussed above and found an age of 8575-840 BC.

According to Scenario 1 from the Altichuelas site, the younger event recorded in the trench corresponds to 1531 AD Baza Eq (Alt\_e4=Baza Eq). This event does not overlap with any of the event PDFs from the Carrizal site (Fig. 7c). Therefore, we propose that this event represents a fault-wide earthquake EQ8 (1531 AD, Baza Earthquake).

Consequently, Earthquake Chronology 1 for the Baza Fault includes eight surface rupturing earthquakes (EQ1 to EQ8) between ca. 45000 BC and 1531 AD (Fig. 7b and 7c), including the Baza Earthquake.

## 5.2 Earthquake chronology 2

Earthquake chronology 2 encompasses the minimum-number-of-events scenario from the Carrizal trench and Scenario 2 from the Altichuelas trench (Fig. 7a).

The overlap analysis of the modelled PDFs for the seven older earthquakes (EQ1 to EQ7) of this earthquake chronology 2 is analogous to that discussed above for earthquake chronology 1 (Fig. 7b and 7d). Differences arise in the younger part of the earthquake chronology. In this case, the youngest event from the Altichuelas trench (Alt\_e4) corresponds with the fault-wide EQ8 (1130-1505 AD). Furthermore, because Scenario 2

of the Altichuelas trench assumes that the Baza Earthquake produced surface rupture (not recorded in the trench), an extra earthquake should be added to the Baza Fault earthquake chronology (EQ9, 1531 AD).

### 5.3 Earthquake chronology 3

Earthquake chronology 3 encompasses the minimum-number-of-events scenario from the Carrizal trench and Scenario 3 from the Altichuelas trench (Fig. 7a).

In this case, the overlap analysis of the modelled PDFs for the eight older earthquakes (EQ1 to EQ8) of this earthquake chronology 3 is equivalent to that discussed above for earthquake chronology 2 (Fig. 7b and 7e). The only difference is that earthquake chronology 3 only involves 8 fault-wide earthquakes, as Scenario 3 of the Altichuelas trench assumes that the Baza Earthquake did not produce surface rupture.

### 5.4 Earthquake chronology 4

Earthquake chronology 4 encompasses the maximum-number-of-events scenario from the Carrizal trench and Scenario 1 from the Altichuelas trench (Fig. 7a).

The overlap analysis indicates that the four older events from the Carrizal site (Car\_e1 to Car\_e4) correspond to the four older fault-wide earthquakes (Fig. 7b and 7f): EQ1 (44260-33215 BC), EQ 2 (33450-24356 BC), EQ 3 (24225-22240 BC), and EQ4 (22220-17539 BC).

When we compare the rupture histories involved in this earthquake chronology 4 (Fig. 7f), we find that event Car\_e5 partially overlaps with three events from the Altichuelas site (Alt\_e1, Alt\_e2, and Alt\_e3). We found a high degree of overlap for the *rupture* Car\_e5=Alt\_e2 (0.41), higher than for the other *ruptures* (Car\_e5=Alt\_e1 overlap 0.28,

Car\_e5=Alt\_e3 overlap 0.24). Moreover, in this earthquake chronology 4, event Car\_e6 partially overlaps with events Alt\_e1, Alt\_e2, and Alt\_e3 (Fig. 7f). The PDF overlap values computed are 0.72 for *rupture* Car\_e6=Alt\_e3, 0.04 for *rupture* Car\_e6=Alt\_e1, and 0.23 for Car\_e6=Alt\_e2. These overlap values led us to propose that (Fig. 7b and 7f) event Alt\_e1 represents earthquake EQ5 (16182-13863 BC). Fault-wide earthquake EQ6 encompasses events Car\_e5 and Alt\_e2 (13790-8845 BC). Earthquake EQ7 includes events Car\_e6 and Alt\_e3 (8485-785 BC).

Finally, the youngest event from the Altichuelas trench (Alt\_e4, Baza Earthquake) corresponds with fault-wide EQ9 (1531 AD, Fig. 7b and 7f)

### 5.5 Earthquake chronology 5

Earthquake chronology 5 encompasses the maximum-number-of-events scenario from the Carrizal trench and Scenario 2 from the Altichuelas trench (Fig. 7a).

The overlap analysis of the seven older earthquakes (EQ1 to EQ7) of earthquake chronology 5 is analogous to that discussed above for earthquake chronology 4 (Fig. 7b and 7g). Differences arise in the younger part of the earthquake chronology; in this case, the youngest event from the Altichuelas trench (Alt\_e4) corresponds with the fault-wide EQ9 (1130-1505 AD). Furthermore, because Scenario 2 of the Altichuelas trench assumes that the Baza Earthquake produced surface rupture, an extra earthquake should be added to the Baza Fault earthquake chronology (EQ10, 1531 AD).

### 5.6 Earthquake chronology 6

Earthquake chronology 6 encompasses the maximum-number-of-events scenario from the Carrizal trench and Scenario 3 from the Altichuelas trench (Fig. 7a).

In this case, the overlap analysis of the modelled PDFs for the eight older earthquakes (EQ1 to EQ8) of earthquake chronology 6 is equivalent to that discussed above for earthquake chronology 5 (Fig. 7b and 7h). The only difference is that earthquake chronology 6 only involves 8 fault-wide earthquakes, as Scenario 3 of the Altichuelas trench assumes that the Baza Earthquake did not produce surface rupture.

The above-discussed PDF overlap analysis indicates that because of the uncertainties of our palaeoseismological data, six different earthquake chronologies can be postulated. These chronologies (Fig 7b) involve between 8 and 9 earthquakes for the time span ca. 45000 BC-1531 AD (earthquake chronologies 1, 2, 4, and 5) or 8 earthquakes for the time span ca. 45000 BC-1505 AD (earthquake chronologies 3 and 6).

## 6 Earthquake recurrence intervals of the Baza Fault

To propose a recurrence interval of the Baza Fault, we analysed the six surface rupturing chronologies discussed above. In all cases, the ages of the postulated earthquakes are expressed in terms of PDF (Fig. 7). To account for these probability functions in the calculation of the recurrence intervals, we used the methodology proposed by DuRoss et al. (2011). We ran six Monte Carlo models. Each model was randomly sampled 10,000 times for each earthquake PDF (previously grouped to 50-year intervals). Each of the 10,000 simulations provided a “random date” for each earthquake. The intervals between these earthquake “random dates” were then used to calculate the elapsed time between pairs of successive earthquakes (e.g., EQ2-EQ1, EQ3-EQ2, etc.). We computed a PDF for the resulting elapsed times by normalizing the frequency of each 50-year interval calculated for each pair of intervals. Finally, we combined the PDF from

pairs of successive earthquakes into a single PDF for each of the six chronologies. We consider these combined PDFs as representative of the earthquake recurrence intervals for the Baza Fault.

All the combined PDFs (Fig. 8) present a broad range of values of possible recurrence interval from 0 to 12000 years (95% confidence) with a multimodal distribution. All the earthquake chronologies present a mode ranging from 4750 to 5150 yr (major mode in chronologies 1, 3, 4, and 6). An older minor mode, varying between 9000 and 9900 yr, is also recognized. Finally, a third mode, ranging from 50 to 100 yr, is present in earthquake chronologies 2 and 5.

The 4750-5150 yr. mode observed in all the chronologies (Fig. 8) is a consequence of the well-constrained elapsed time between earthquake pairs EQ3-EQ4, EQ4-EQ5, and EQ5-EQ6. Analogously, the 9000-9900 yr. mode is a consequence of the wide range of elapsed time between earthquake pairs EQ1-EQ2, EQ2-EQ3, EQ6-EQ7 and EQ7-EQ8. In earthquake chronologies 2 and 5, the 50-100 yr. mode is biased by the time lapse calculated between the penultimate earthquake and the 1531 Baza Earthquake (Fig. 8), since the PDF is strongly conditioned by the perfectly constrained occurrence of this last earthquake (its age is not a PDF, only a point, 1531 AD). Consequently, this youngest mode is partially an artefact related to data heterogeneity. Moreover, the 50-100 yr. mode is also a consequence of the assumption that the Baza Earthquake produced surface rupture but was not recorded in the Artichuelas site. This small recurrence interval is completely out of range of the values within the region, so we consider that as an evidence to reject the assumption above mentioned.

The two older modes can be explained by assuming a perfect characteristic earthquake model (cf. Shimazaki and Nakata, 1980), i.e., by assuming a constant periodic pattern for the Baza Fault. We postulate that the oldest mode (9000-9900 yr., Fig. 8) represents twice the second-oldest mode (4750-5150 yr.). Therefore, because the time elapsed PDFs between all consecutive pairs of earthquakes from EQ3 to EQ6 are within the range of the second-oldest mode (Fig. 8), we hypothesise that the palaeoseismological record of the first group of chronologies could be considered complete between EQ3 and EQ6. The recurrence interval PDFs before EQ3 and after EQ6 are responsible for the oldest mode (which is twice the second-oldest mode, as mentioned above). Hence, we propose that one event is missing between EQ1-EQ2, EQ2-EQ3, and EQ6-EQ7.

## 7 Single event displacement

In this section, we discuss the single event displacement deduced from our above-presented results (recurrence intervals) and the long-term slip rates of the Baza Fault. We compare these data with the per-event displacement deduced by using empirical relationships.

Our new palaeoseismological data of the Baza Fault seem to indicate that the RIs of the surface-rupturing earthquakes range between 4750-5150 yr. Previous studies indicate that the long-term (Middle Pleistocene) vertical slip rate of the fault varies between 0.17 and 0.49 mm/yr (García-Tortosa et al., 2011). These slip rate values are derived from the offset of a geomorphic surface. Different ages have been proposed for this surface, ranging between 205 and 600 kyr. (Scott and Gibert, 2009; Díaz-Hernández and Juliá, 2006; see discussion in García Tortosa et al., 2011). Accounting for the 45°-60° of general

dip and the pure dip-slip kinematics of the Baza Fault (Alfaro et al., 2008), we estimate a net slip rate between 0.20 and 0.69 mm/yr.

We use different empirical regressions to evaluate the relationship between per-event displacement and rupture length (although this regression presents high uncertainties). As previously discussed, considering the maximum rupture length of the Baza Fault, we obtained an average per-event displacement (AD) of 0.78-0.90  $\pm$ 0.37 m and a maximum per-event displacement (MD) of 2.06-2.44  $\pm$ 0.41 m by using the Wells and Coppersmith (1994) regressions. The regression proposed by Stirling et al. (2002) yielded an AD of 2.15-2.20  $\pm$ 0.24 m. By multiplying these values by the above-mentioned long-term slip rate, we obtain a theoretical recurrence interval ranging between ca. 1300 and 10300 yr. These values are compatible with the RI we calculated from our palaeoseismological analysis.

Moreover, if we multiply the above-presented RI (4750-5150 yr.) by the long-term Middle Pleistocene slip rates of the Baza Fault (0.20 and 0.69 mm/yr, after Alfaro et al., 2008), we obtain a theoretical single event displacement ranging between ca. 0.9 and 3.6 m (assuming that all of the fault offset is produced by surface-rupturing events). We observe that the displacement values obtained from trenches observation are within the range of those derived from the empirical regressions. Analogously, our RI values are also within the range of the RI derived from the empirical regressions, as above mentioned. Consequently, we consider this agreement as further support to the RI we obtained.

## 8 Conclusions

The first Palaeoseismic results of the Baza fault, one of the most significant active normal faults of the central Betic Cordillera, permit us to deduce a variable number of palaeoseismic events. These events were identified in two trenches excavated in the central and southern sectors of the fault (the Carrizal trench and the Altichuelas trench, respectively). Five or six surface rupturing events were identified in the Carrizal trench during the last ca. 45000 yr. Four events were recorded in the Altichuelas trench since ca. 16000 yr BC. The ages of all these events have been constrained by a detailed Bayesian statistical analysis using Oxcal software.

From these events, we postulate different fault-wide earthquake chronologies of the Baza fault. We consider up to six different earthquake chronologies, because of uncertainties related to both geological features and dating. These chronologies invoke between 8 and 9 surface-rupturing earthquakes in the last ca. 45000 yrs.

In addition, six Monte Carlo simulations provide a recurrence interval of the Baza Fault ranging between 4750 and 5150 yr, depending on the earthquake chronology considered.

We compare these results with different palaeoseismic parameters of the Baza Fault obtained from empirical regressions. The agreement observed between our calculations and the empirical regressions further support our analysis.

Although we consider the presented results as robust and reliable (accounting for the uncertainties discussed) we think that further palaeoseismic analyses are necessary to better constrain the palaeoseismic parameters of the Baza Fault.



## 9 Acknowledgements

Funding: This research was founded by the Spanish Ministry of Economics, Industry and Competitiveness (MINECO) research Projects CGL2011- 30153-C02-02 and EPILATES (CGL2015-65602-R). Also by the research group VIGROB053 (University of Alicante), the research Project UJA2014/06/17 (Caja Rural de Jaén and University of Jaen) and the research contract 2015CL015 (University of Jaen).

## 10 References

- Agusti, J., Oms, O., Remacha, E., 2001. Long Plio-Pleistocene terrestrial record of climate change and mammal turnover in Southern Spain. *Quaternary Research* 56, 411-418.
- Alfaro, P., Moretti, M., Soria, J.M., 1997. Soft-sediment deformation structures induced by earthquakes (seismites) in pliocene lacustrine deposits (Guadix-Baza Basin, Central Betic Cordillera). *Eclogae Geol Helv* 90: 531–540.
- Alfaro, P., Galindo-Zaldívar, J., Jabaloy, A., López-Garrido, A.C., Sanz de Galdeano, C., 2001. Evidence for the activity and Palaeoseismicity of the Padul fault (Betic Cordillera, southern Spain). *Acta Geológica Hispánica* 36 (3-4), 283-295.
- Alfaro, P., Delgado, J., Sanz de Galdeano, C., Galindo Zaldívar, J., García Tortosa, F.J., López Garrido, A.C., López Casado, C., Marín, C., Gil, A.J., Borque, M.J., 2008. The Baza Fault: a major active extensional fault in the central Betic Cordillera (South Spain). *International Journal of Earth Sciences* 97, 1353-1365. doi:10.1007/s00531-007-0213-z

Alfaro, P., Gibert, L., Moretti, M., García-Tortosa, F.J., Sanz de Galdeano, C., Galindo-Zaldívar, J., López-Garrido, A.C., 2010. The significance of giant seismites in the Plio-Pleistocene Baza palaeolake (S Spain). *Terra Nova* 22 (3), 172–179. doi:10.1111/j.1365-3121.2010.00930.x

Berryman, K., Villamor, P., Nairn, I., Van Dissen, R., Begg, J., Lee, J., 2008. Late Quaternary surface rupture history of the Paeroa Fault, Taupo Rift, New Zealand. *New Zealand Journal of Geology and Geophysics*, 51, 135–158.

Biasi, G. P., Weldon, R. J., 2009. San Andreas Fault rupture scenarios from multiple Palaeoseismic records: Stringing pearls, *Bull. Seismol. Soc. Am.* 99, no. 2A, 471–498, doi 10.1785/0120080287.

Bronk Ramsey, C. 2009a. Bayesian analysis of radiocarbon dates. *Radiocarbon*, 51(1), 337-360.

Bronk Ramsey, C., 2009b. Dealing with outliers and offsets in radiocarbon dating. *Radiocarbon*, 51(3), 1023-1045.

Bronk Ramsey, C., 2010. OxCal 4.1 Manual, [http://c14.arch.ox.ac.uk/oxcalhelp/hlp\\_contents.html](http://c14.arch.ox.ac.uk/oxcalhelp/hlp_contents.html) (last accessed December 2016).

Calvache, M.L., Viseras, C., Fernández, J., 1997. Controls on fan development-evidence from fan morphometry and sedimentology; Sierra Nevada, SE Spain. *Geomorphology* 21, 69-84. doi:10.1016/S0169-555X(97)00035-4

De Vicente, G., Cloetingh, S., Muñoz, A., Olaiz, A., Stich, D., Vegas, R., Galindo-Zaldívar, J., Fernández, J., 2008. Inversion of moment tensor focal mechanisms for active stresses around the microcontinent Iberia: Tectonic implications. *Tectonics*, 27, TC1009. doi: 10.1029/2006TC002093.

Díaz-Hernández, J.L., Juliá, R., 2006. Geochronological position of badlands and geomorphological patterns in the Guadix–Baza basin (SE Spain). *Quaternary Research* 65, 467–477.

DuRoss, C.B., Personius, S.F., Crone, A.J., Olig, S.S., Lund, W.R., 2011. Integration of Palaeoseismic Data from Multiple Sites to Develop an Objective Earthquake Chronology: Application to the Weber Segment of the Wasatch Fault Zone, Utah. *Bulletin of the Seismological Society of America*, vol. 101 no. 6 2765-2781, DOI: 10.1785/0120110102

Estévez, A., Sanz de Galdeano, C., 1983. Néotectonique du secteur central des Chaînes Bétiques (Basins du Guadix-Baza et de Grenade). *Rev. Géogr. Phys. Géol. Dynam.*, 21, 23-34.

Galindo-Zaldívar J., González-Lodeiro F., Jabaloy A., 1993. Stress and palaeostress in the Betic-Rif Cordilleras (Miocene to Present). *Tectonophysics* 227:105–126

García Tortosa, F.J., Alfaro, P., Galindo Zaldívar, J., Gibert, L., López Garrido, A.C., Sanz de Galdeano, C., Ureña, M., 2008. Geomorphologic evidence of the active Baza fault (Betic Cordillera, South Spain). *Geomorphology* 97, 374-391. doi: 10.1016/j.geomorph.2007.08.007

García Tortosa, F.J., Alfaro, P., Galindo Zaldívar J., Sanz de Galdeano, C., 2011. Glacis geometry as a geomorphic marker of recent tectonics: the Guadix-Baza Basin (South Spain). *Geomorphology* 125, 517-529. doi: 10.1016/j.geomorph.2010.10.021

Gibert, L., Ortí, F., Rosell, L., 2007. Plio-Pleistocene lacustrine evaporites of the Baza Basin (Betic Chain, SE Spain). *Sedimentary Geology* 200, 89-116. doi:10.1016/j.sedgeo.2007.03.003

Gil, A.J., Rodríguez-Caderot, G., Lacy, M.C., Ruiz, A.M., Sanz de Galdeano, C., Alfaro, P., 2002. Establishment of a non-permanent GPS network to monitor the recent deformation in the Granada Basin (Betic Cordillera, Southern Spain). *Studia Geophysica et Geodaetica* 46, 395–410.

Goodfriend, G.A., Stipp, J.J., 1983. Limestone and the problem of radiocarbon dating of land snail shell carbonate: *Geology*, v 11, no. 10, p 575-577.

Haberland, C., Gibert, L., Jurado, M.J., Stiller, M., Baumann-Wilke, M., Scott, G.; Mertz, D.F., 2017. Architecture and tectono-stratigraphic evolution of the intramontane Baza Basin (Béticos, SE-Spain): Constraints from seismic imaging. *Tectonophysics*, 709, 69-84.

Herráiz, M., De Vicente, G., Lindo-Naupari, R., Giner, J., Simón, J.L., González-Casado, J.M., Vadillo, O., Rodríguez-Pascua, M.A., Cicuéndez, J.I., Casas, A., Cabañas, L., Rincón, P., Cortés, A.L., Ramírez, M., Lucini, M., 2000. The recent (upper Miocene to Quaternary) and present tectonic stress distributions in the Iberian Peninsula. *Tectonics*, 19, 762-786.

IGME (2015). QAFI v.3: Quaternary Active Faults Database of Iberia. <http://info.igme.es/QAFI> (accessed 28 August 2017).

IGN – Instituto Geográfico Nacional (2015). Catálogo de terremotos (Earthquakes catalog). <http://www.ign.es/ign/layoutIn/sismoFormularioCatalogo.do> (accessed 13 August 2017).

Lhénaff, R., 1965. Néotectonique quaternaire sur le bord occidental de la Sierra Nevada (province de Grenade, Espagne). *Revue de Géographie Physique et de Géologie Dynamique* 2 (VII/3), 205-207.

Martín, R., Stich, D., Morales, J., Mancilla, F., 2015. Moment tensor solutions for the Iberian-Maghreb region during the IberArray deployment (2009-2013). *Tectonophysics*, 663 (16), 261-274.

Martínez-Solares, J.M., Mezcua, J., 2003. Catálogo sísmico de la Península Ibérica (880 AC-1900). Monografía nº 18 Instituto Geográfico Nacional, Madrid, Spain, pp 1–254

Martínez Solares, J.M., Cabañas Rodríguez, L., Benito Oterino, M.B., Rivas Medina, A., Gaspar Escribano, J.M., Ruíz Barajas, S., Rodríguez Zaloña, O., 2013. Actualización de mapas de peligrosidad sísmica de España 2012. Centro Nacional de Información Geográfica, Madrid, 267 p.

McCalpin, J., 2009. Palaeoseismology. Burlington, MA: Academic Press. 613 p.

Mercier, J.-L., Carey-Gailhardis, E., Mouyaris, N., Simeakis, K., Roundoyannis, T., and Anghelidhis, C., 1983. Structural analysis of recent and active faults and regional state of stress in the epicentral area of the 1978 Thessaloniki earthquakes (northern Greece). *Tectonics* 2, 577-600.

Muñoz, D., Udías, A., 1991. Three large historical earthquakes in Southern Spain. En: J. Mézcua and A. Udías (eds.), *Seismicity, Seismotectonics and Seismic Risk of the Ibero-Maghrebian Region*. Publ. Inst. Geogr. Nac., 8, Madrid, 175-182.

Nocquet, J.M., 2012. Present-day kinematics of the Mediterranean: a comprehensive overview of GPS results. *Tectonophysics*, 579, 220-242.

Peña, J.A., 1985. La depresión de Guadix-Baza. *Estudios Geológicos* 41:33–46

Reicherter, K.R., Jabaloy, A., Galindo-Zaldívar, J., Ruano, P., Becker-Heidmann, P., Morales, J., Reiss, S., González-Lodeiro, F., 2003. Repeated palaeoseismic activity of the Ventas de Zafarraya fault (S Spain) and its relation with the 1884 Andalusian earthquake. *Int. J. Earth Sci.*, 92, 912-922.

Reiter, L., 1990. Earthquake Hazard Analysis: Issues and Insights, Columbia University Press, New York. 254 p.

Reiter, L., 1995. Palaeoseismology. A user's perspective. In (Editors L. Selva and L.B. Slemmons) Perspectives in Palaeoseismology. Assoc. Eng. Geol. Spec. Pub. Vol 6, p 3-6.

Riley, C., Moore, J. McM., 1993. Digital elevation modelling in a study of the neotectonic geomorphology of the Sierra Nevada, southern Spain. *Zeitschrift für Geomorphologie*, 94, 25-39.

Rodríguez-Fernández, J.C., Sanz de Galdeano, C., 2006. Late orogenic intramontane basin development: the Granada basin, Betics (southern Spain). *Basin Research*, 18, 85-102.

Ruiz, A.M., Ferhat, G., Alfaro, P., Sanz de Galdeano, C., Lacy, M.C., Rodríguez-Caderot, G., Gil, A.J., 2003. Geodetic measurement of crustal deformation on NW-SE faults of the Betic Cordillera, Southern Spain, 1999-2001. *Journal of Geodynamics*, 35, 259-272.

Sanz de Galdeano, C., García-Tortosa, F.J., Peláez, J.A., Alfaro, P., Azañón, J.M., Galindo-Zaldívar, J., López-Casado, C., López-Garrido, A.C., Rodríguez-Fernández, J., Ruano, P., 2012. Main active faults in the Granada and Guadix-Baza Basins (Betic Cordillera). *Journal of Iberian Geology*, 38 (1), 209-223.

Sanz de Galdeano, C., Peláez, J.A., 2011. Fallas activas en la Cordillera Bética. Una aproximación a partir de la información tectónica y sísmica. Editorial Universidad de Granada, 287 p.

Scott, G., Gibert, L., 2009. The oldest hand-axes in Europe. *Nature* 461, 82–85.

Shimazaki, K., Nakata, T., 1980. Time-predictable recurrence model or large earthquakes, *Geophys. Res. Lett.*, 7, 279–282.

Stich, D., Serpelloni, E., Mancilla, F., Morales, J., 2006. Kinematics of the Iberia-Maghreb plate contact from seismic moment tensors and GPS observations. *Tectonophysics*, 426, 295-317.

Stirling, M., Rhoades, D., Berryman, K., 2002. Comparison of earthquake scaling relations derived from data of the instrumental and preinstrumental era. *Bulletin of the Seismological Society of America*.

Stirling, M., Goded, T., Berryman, K., Litchfield, N., 2013. Selection of earthquake scaling relationships for seismic-hazard analysis. *Bull. Seismol. Soc. Am.*, 103, 2993-3011.



Vera, J.A., 1970. Estudio estratigráfico de la depresión de Guadix–Baza. *Boletín Geológico y Minero*, 91, 429-462.

Wells, Donald & Coppersmith, K., 1994. New Empirical Relationships among Magnitude, Rupture Length, Rupture Width, Rupture Area, and Surface Displacement. *Bulletin of the Seismological Society of America*. 84. 974-1002.

## FIGURE CAPTIONS

Figure 1: a) Geological sketch map of the Betic Cordillera (legend as in figure b). b) General geological map of the Baza Fault.

Figure 2: a) Geological cross section along the Carrizal sector and across the Baza Fault. Note how offsets observed in the Pleistocene units indicate that most of the cumulative slip of the Baza Fault concentrates along two main strands. b) Geological–geomorphological map of the Carrizal sector, where the Carrizal trench was excavated.

Figure 3: a and b) Carrizal trench logs. See Figure 2 for location. Inset in a shows the tilt of the different layers c) Interpretation in terms of palaeoseismic stratigraphic sequences and events. Green circles with grey labels, non-dated radiocarbon samples, yellow circles with black labels, dated samples. Strikethrough grey labels indicate dated samples not considered.

Figure 4: a) Geological–geomorphological map of the Altichuelas sector, where the Altichuelas trench was excavated. b) Topographic profile across the Altichuelas trench. Position of the main geomorphic features are indicated. Location in figure 4a.

Figure 5: a and b) The Altichuelas trench logs. See Figure 4 for location. Interpretation in terms of Palaeoseismic stratigraphic sequences and events is also included. Green circles with grey labels, non-dated radiocarbon samples, yellow circles with black labels, dated samples. Yellow stars, OSL samples. Strikethrough grey labels indicate dated samples not considered. c) Logic trees showing the different hypotheses discussed for the plaeoseismic interpretation.

Figure 6: Correlation of wall PDFs from OxCal models for the Altichuelas trench. a) Logic tree showing the different scenarios discussed for the palaeoseismic interpretation. b, c, and d) Scenarios 1, 2, and 3, respectively. Colour bars show how walls PDFs correlate to form site earthquakes Alt\_e1 to Alt\_e4. Horizontal bars show 95% confidence interval. Note the different vertical scale for AltN\_e3, Alt\_e4, and the last events of all trenches (probability=1, historical event).

Figure 7: Correlation of site PDFs for the Baza Fault palaeoseismic sites. a) Scheme showing the six Earthquake Chronologies discussed. b) Resumed ages of the Earthquake Chronologies. c to h) Earthquake chronologies 1 to 6. Colour bars show how site PDFs correlate to form fault earthquakes EQ1 to EQ9. Horizontal bars show 95% confidence interval. Note the different vertical scale for Baza Earthquake in chronologies 1, 2, 4, and 5 (probability=1, historical event).

Figure 8: Analysis of the Baza Fault EQ recurrence. Each column of graphics shows PDFs for the lapse time between pairs of consecutive earthquakes (i.e.: EQ2-EQ1, EQ3-EQ2, etc.) for the considered chronologies. The bottom row shows the combined PDF of recurrence intervals by adding all the random values from pairs of consecutive earthquakes for each chronology, highlighting a multimodal pattern. Axes parameters and scale are equal for all graphics.

Table 1

Radiocarbon samples								
Sample	Trench	Radiocarbon age		Calibrated age	$\delta(^{13}\text{C})$	Fraction of modern		Lab. Code
		BP	1 $\sigma$ error		per mil	pMC	1 $\sigma$ error	
<b>ALT-N12</b>	Altichuelas	13261	52	<b>14177-13797 BC</b>	-22.7	0.192	0.0012	NZA 61822
<b>ALTS-08</b>	Altichuelas	9468	40	<b>9113-8630 BC</b>	-24.7	0.308	0.0015	NZA 61342
<b>CAR-C2-S</b>	Carrizal	2473	22	<b>750-405 BC</b>	-18	73.5	0.2	D-AMS 012180
<b>CAR-N10</b>	Carrizal	618	29	<b>1313-1423 AD</b>	-23.8	92.6	0.34	D-AMS 012182
<b>CAR-N12</b>	Carrizal	38806	372	<b>41312-40247 BC</b>	-17.8	0.798	0.037	D-AMS 012183
<b>CAR-N15</b>	Carrizal	527	29	<b>1406-1452 AD</b>	-21.2	93.65	0.34	D-AMS 012184
<b>CAR-N17</b>	Carrizal	21878	169	<b>26493-25813 BC</b>	-24	0.066	0.0014	NZA 61417
<b>CAR-N2</b>	Carrizal	20305	120	<b>22877-22108 BC</b>	-23.6	0.08	0.0012	NZA 61824
<b>CAR-N4</b>	Carrizal	31745	205	<b>34185-33190 BC</b>	-17.5	1.922	0.049	D-AMS 010840
<b>CAR-N8</b>	Carrizal	20176	118	<b>22582-21993 BC</b>	-24.1	0.081	0.0012	NZA 61823
<b>CAR-S4</b>	Carrizal	16086	77	<b>17643-17167 BC</b>	-14.9	13.5	0.13	D-AMS 012181
OSL samples								
Sample	Trench	Depth (m)	Moisture (%)	Dose rate (Gy/ka)	Equivalent dose (Gy)	Age (ka before 2015)		
<b>ALTN-03</b>	Altichuelas	2	5	2.4 $\pm$ 0.1	40.1 $\pm$ 2.2	<b>16.9<math>\pm</math>1.1</b>		
<b>ALTN-60</b>	Altichuelas	1	5	2.19 $\pm$ 0.1	1.8 $\pm$ 0.2	<b>0.8<math>\pm</math>0.1</b>		
<b>ALTN-61</b>	Altichuelas	0.5	5	2.35 $\pm$ 0.08	22.9 $\pm$ 1.1	<b>9.8<math>\pm</math>0.6</b>		
<b>ALTS-50</b>	Altichuelas	1.2	5	1.86 $\pm$ 0.06	1.8 $\pm$ 0.2	<b>0.95<math>\pm</math>0.11</b>		
<b>ALTS-51</b>	Altichuelas	1.4	5	2.04 $\pm$ 0.1	3.1 $\pm$ 0.4	<b>1.53<math>\pm</math>0.2</b>		
<b>ALTS-52</b>	Altichuelas	1.4	5	1.99 $\pm$ 0.06	5.4 $\pm$ 0.6	<b>2.7<math>\pm</math>0.3</b>		
<b>ALTS-53</b>	Altichuelas	1.2	5	2.13 $\pm$ 0.07	2.2 $\pm$ 0.3	<b>1.02<math>\pm</math>0.13</b>		

**Highlights**

The first palaeoseismic analysis of the Baza Fault (SE Spain) is presented

We postulate six alternative fault-wide surface rupturing histories for the Baza fault

Chronologies suggests 8-9 surface-rupturing earthquakes in the last ca. 45000 yr

Recurrence interval of the Baza Fault is 4750-5150 yr

Results agree with palaeoseismic parameters obtained from empirical regressions

ACCEPTED MANUSCRIPT

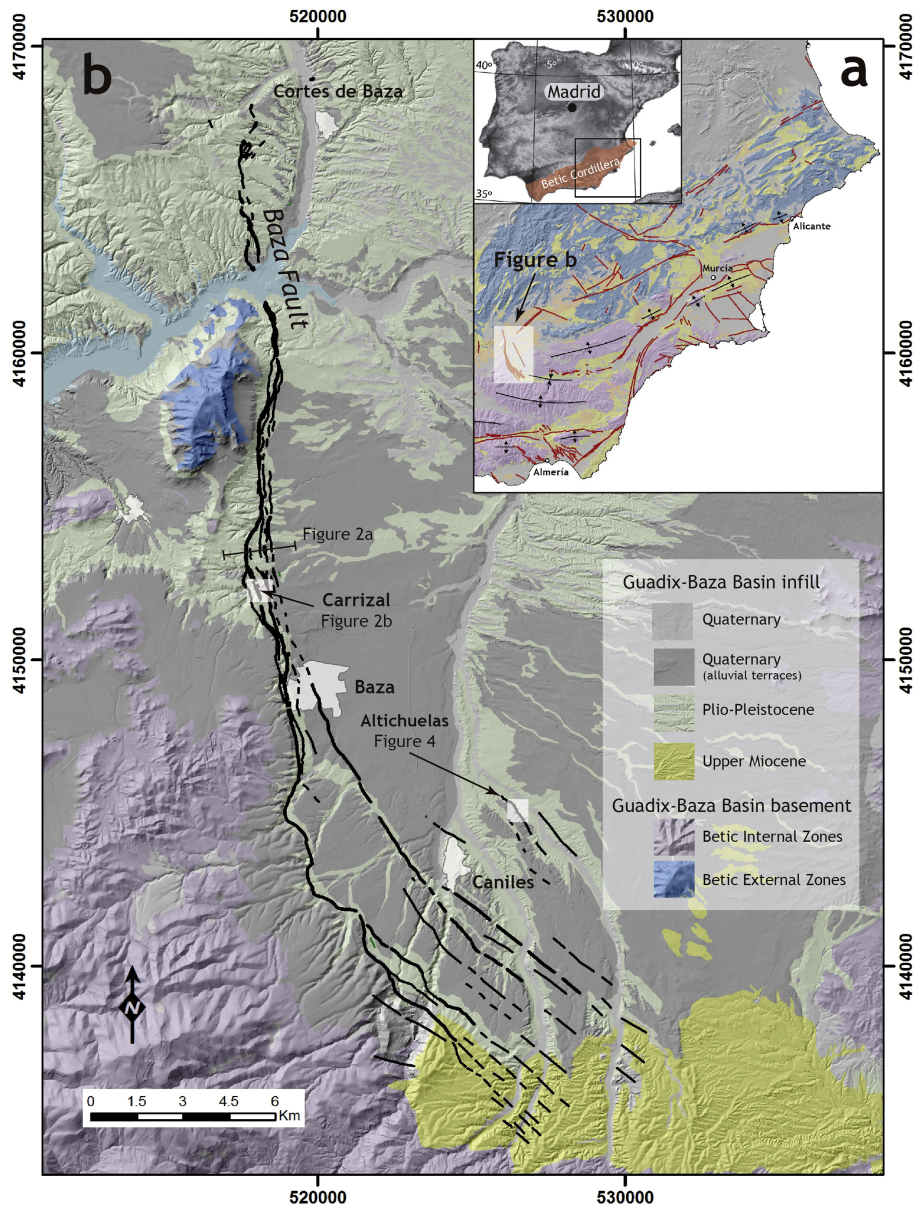


Figure 1

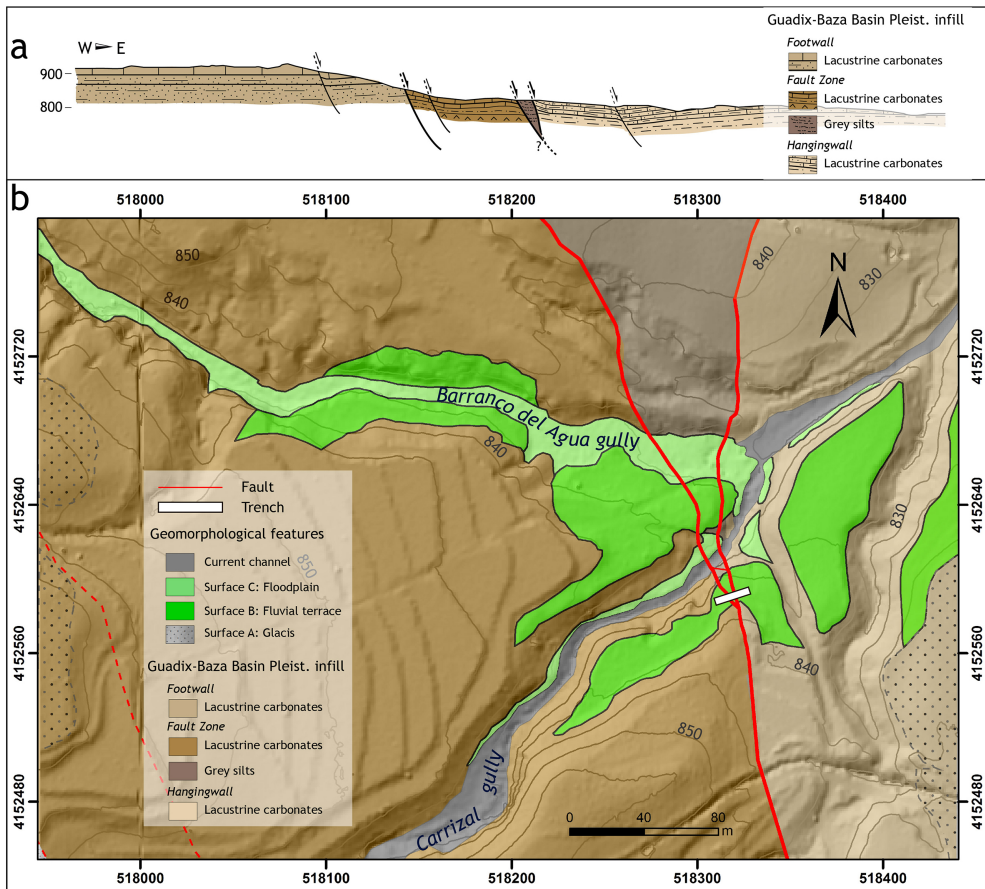


Figure 2

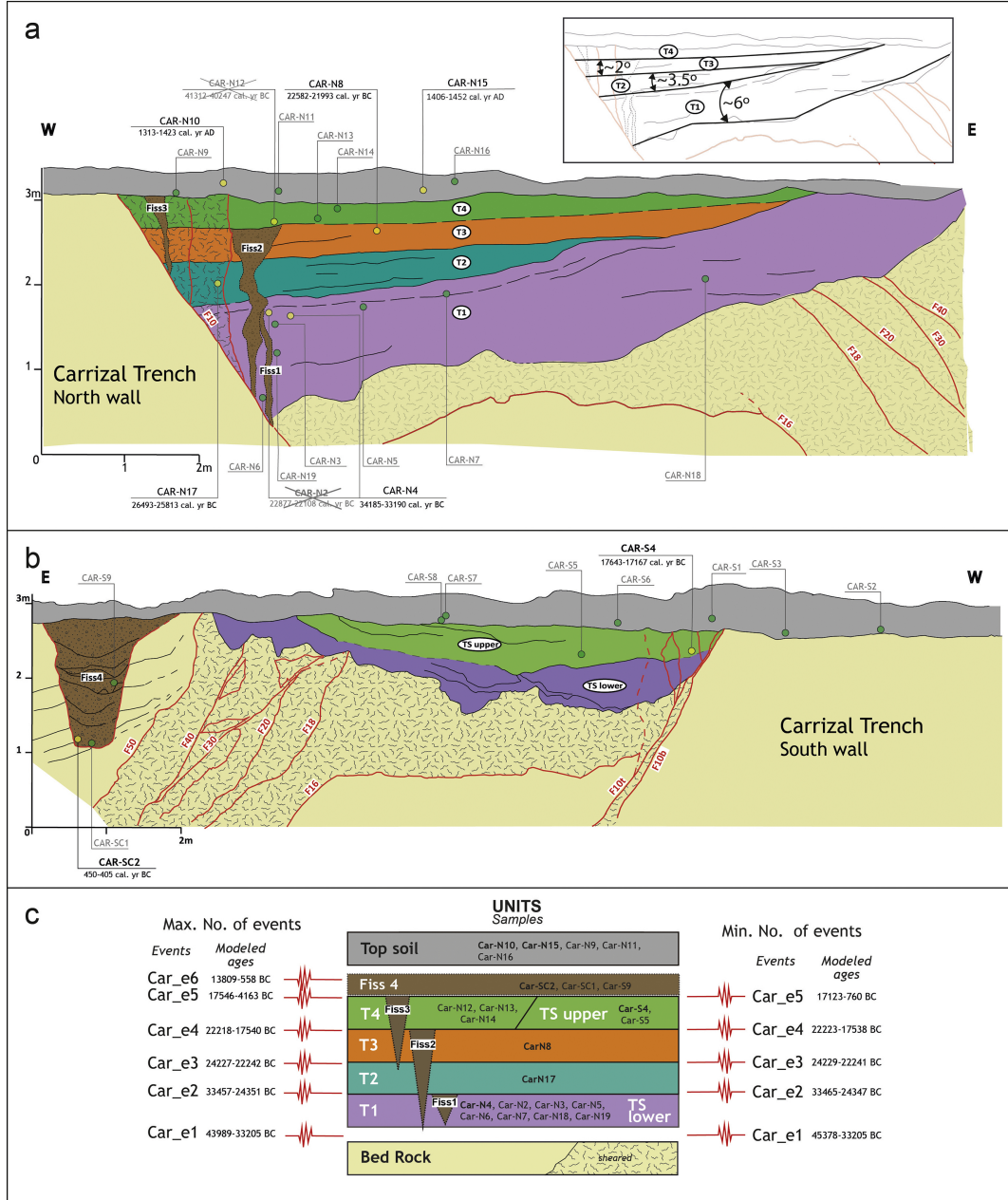


Figure 3



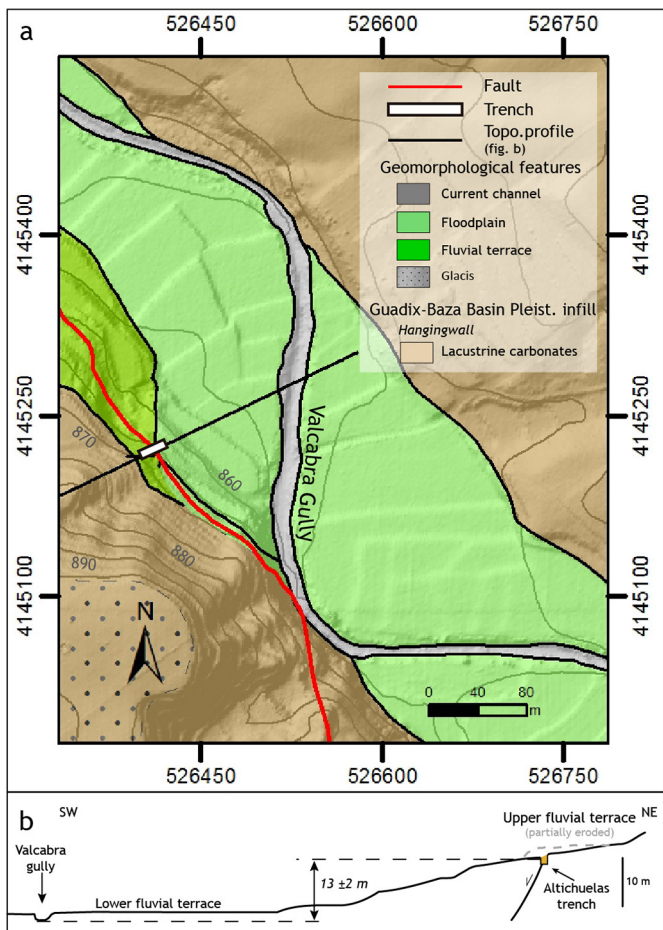


Figure 4

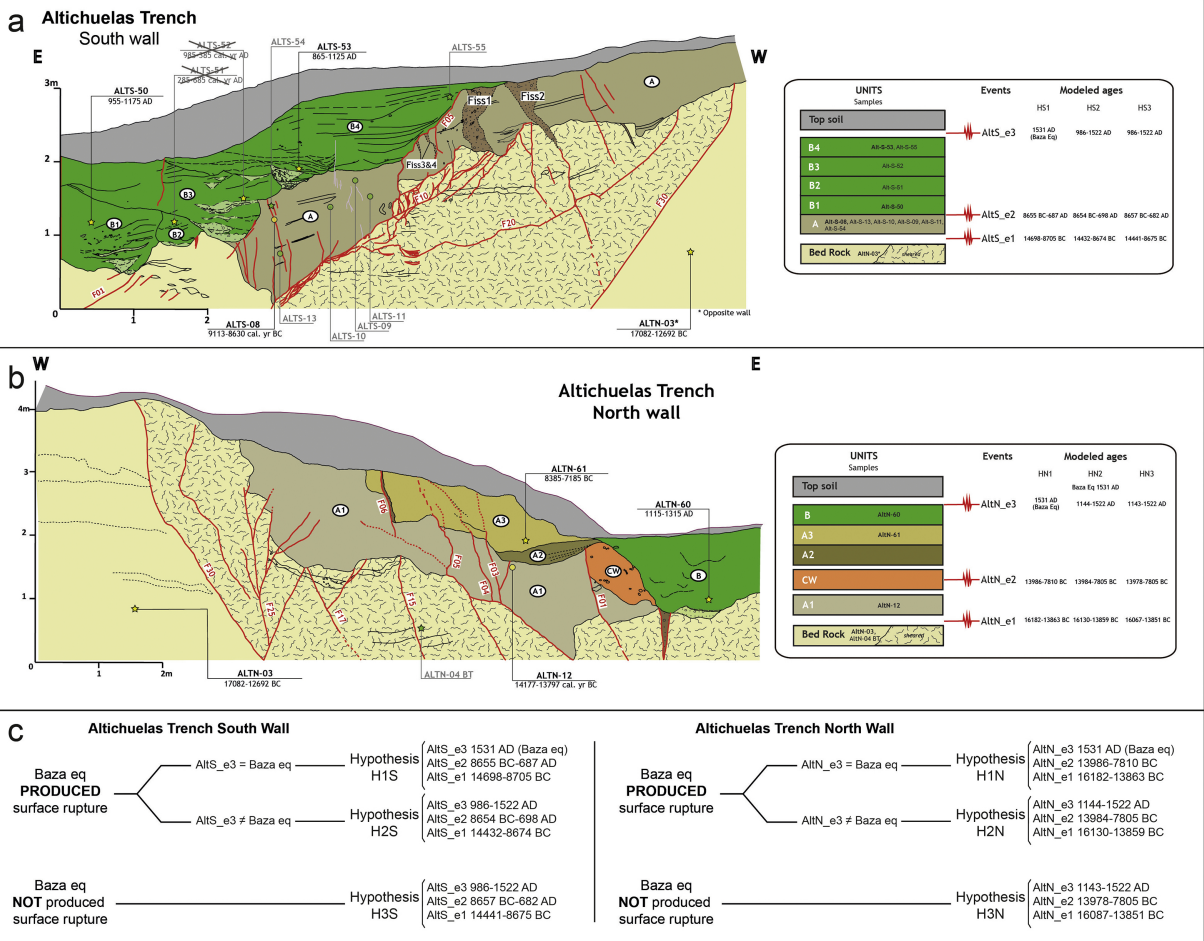


Figure 5

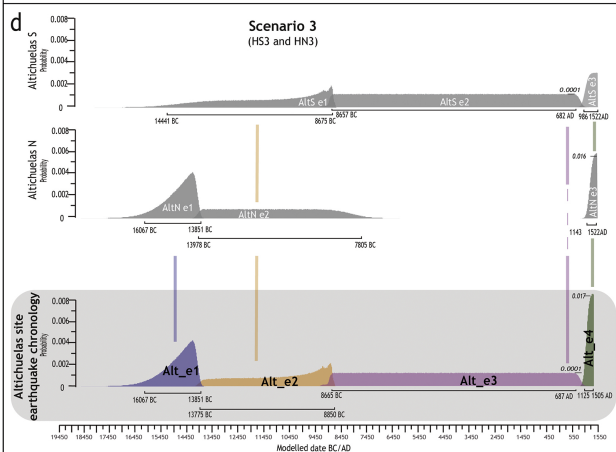
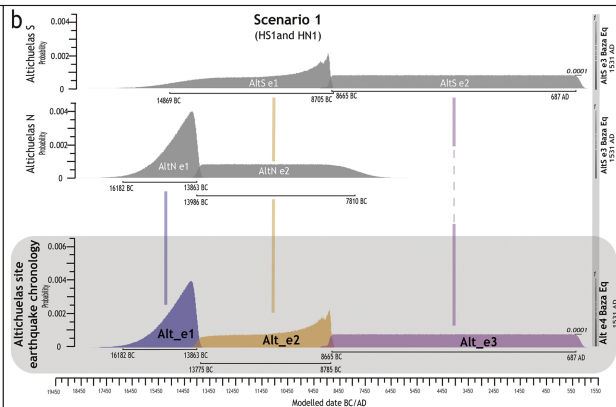
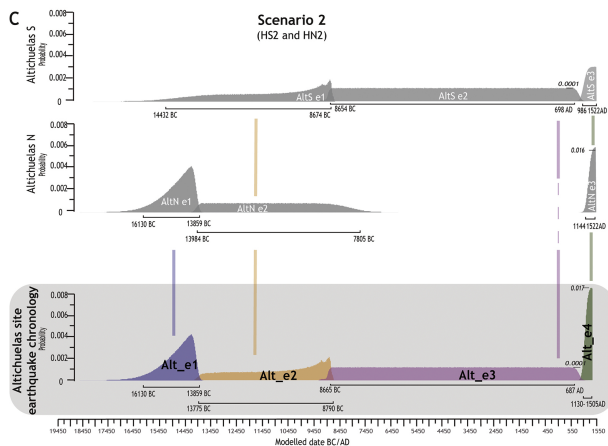
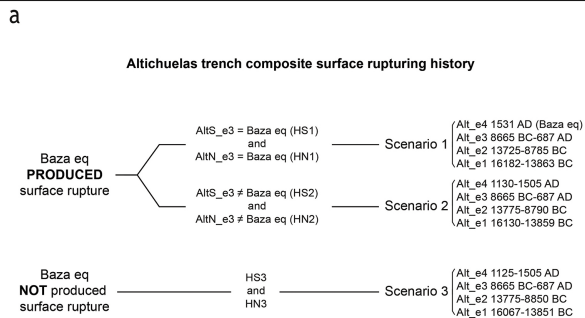


Figure 6

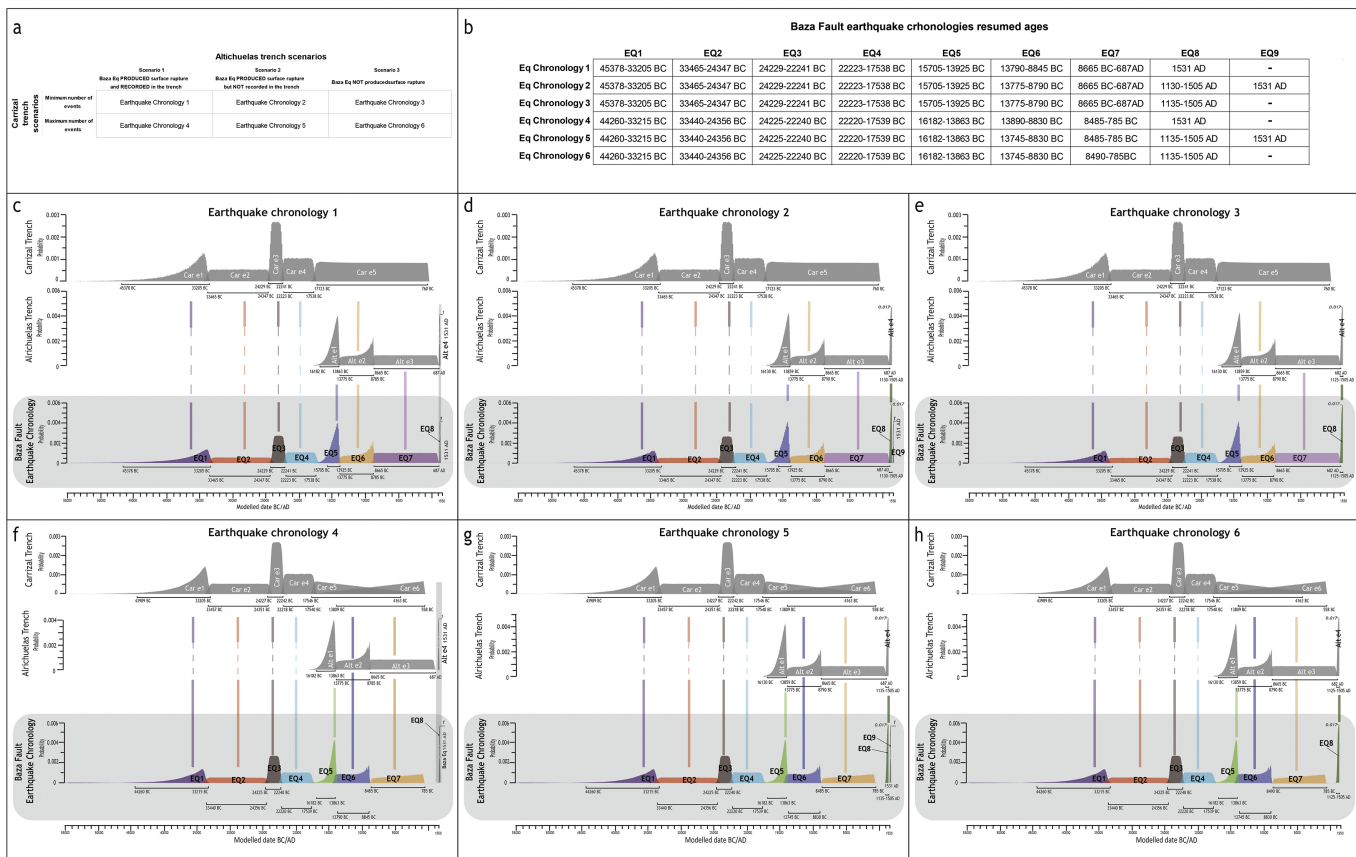


Figure 7

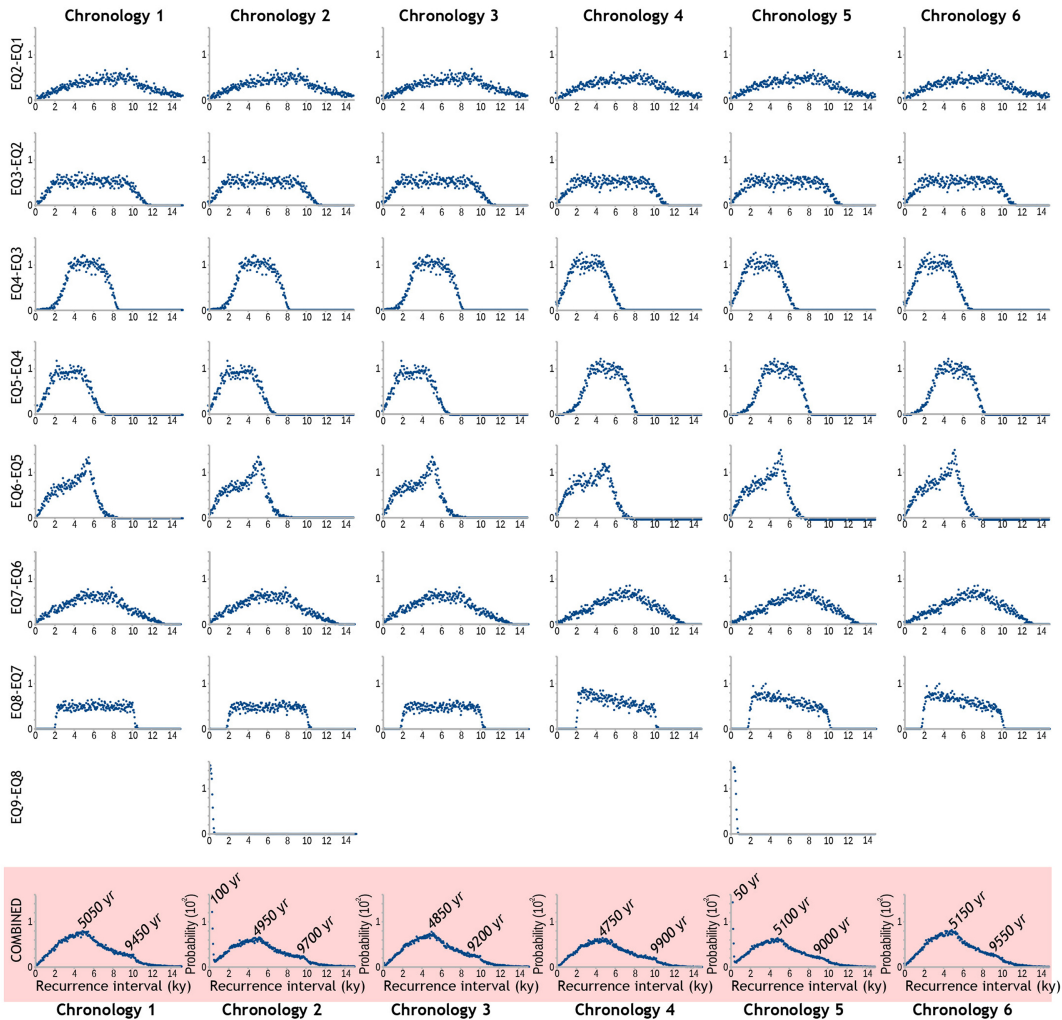


Figure 8